

Politecnico di Torino

Politecnico di Torino

Corso di Laurea Magistrale in Ingegneria Energetica e Nucleare

Anno Accademico 2025/2026

AC Losses in High-Temperature Superconducting Magnets

Experimental Investigation, FEM Modeling, and Mitigation via Striated REBCO Tapes

Relatori:
Prof.ssa Laura Savoldi

Candidati:
Paolo Guidi

Table of Contents

List of Figures VI

1 Introduction 3
- 1.1 Goal of the Thesis . . . 4
- 1.2 Structure of the Thesis . . . 4

2 Case study - Experiment description 6
- 2.1 Coil geometry description . . . 7
  - 2.1.1 Pancake parameters . . . 7
  - 2.1.2 Tape description . . . 8
  - 2.1.3 Coil supports . . . 10
  - 2.1.4 Instrumentation . . . 12
- 2.2 Preliminary analysis . . . 14
  - 2.2.1 Critical current . . . 14
  - 2.2.2 Inductance . . . 16
- 2.3 Experiment . . . 16
- 2.4 Results . . . 17
  - 2.4.1 Magnetic field . . . 17
  - 2.4.2 Potential difference . . . 19
  - 2.4.3 Energy dissipated . . . 20

3 Computational FEM simulation 22
- 3.1 Simulation setup . . . 22
  - 3.1.1 Simulation geometry . . . 22
  - 3.1.2 Models . . . 24
  - 3.1.3 Mesh . . . 25
- 3.2 Simulation parameters . . . 27
  - 3.2.1 Critical current . . . 27
  - 3.2.2 Electrical resistivity . . . 28
  - 3.2.3 RRR measurement . . . 30
- 3.3 Uncertainty quantification . . . 31

3.3.1 Numerical uncertainty . . . 31
3.3.2 Input data uncertainty . . . 34
3.4 Results . . . 35
3.4.1 Maximum current 300 A . . . 35
3.4.2 Maximum current 400 A . . . 36
3.4.3 Maximum current 500 A . . . 39

4 Analytical simulations 44
4.1 Equations . . . 44
4.2 Parameter determination . . . 45
4.2.1 Electrical resistance . . . 45
4.2.2 Magnetic inductance . . . 46
4.2.3 Mutual inductance coefficient . . . 47
4.3 Model solution . . . 47
4.4 Results . . . 48
4.4.1 Maximum current 300 A . . . 49
4.4.2 Maximum current 400 A . . . 51
4.4.3 Maximum current 500 A . . . 53

5 Analytical formulations for AC losses 56
5.1 Analytical method for magnetic field evaluation . . . 56
5.2 Hysteresis losses . . . 58
5.2.1 Kajikawa method . . . 58
5.2.2 Comparison with experiments . . . 59

6 Possible strategy for AC losses mitigation: striated tapes 61
6.1 AC loss contributions in striated conductors . . . 62
6.1.1 Hysteresis losses . . . 63
6.1.2 Eddy-current losses . . . 64
6.1.3 Coupling losses . . . 64
6.1.4 Critical length . . . 66
6.2 HTS striated tapes fabrication . . . 67
6.2.1 Striation after REBCO . . . 67
6.2.2 Striation before REBCO . . . 68
6.2.3 Current redistribution in striated tapes . . . 69

7 Case study: Subra HTS striated tape 71
7.1 Fabrication method: the 2LUPS technique . . . 71
7.1.1 Fabrication steps . . . 71
7.1.2 2LUPS advantages . . . 72
7.2 Critical current comparison . . . 73
7.2.1 Critical current measurement: experiment . . . 73

7.2.2 Critical current measurement: results 74
7.3 Striated tape: numerical simulations 77
7.3.1 Simulations setup 77
7.3.2 Results 78

8 Conclusion and Outlook 82
8.1 Summary of Main Results 82
8.2 Future steps 84

Bibliography 85

List of Figures

2.1 Upper view of the pancake coil 8
2.2 scheme of an HTS tape. 9
2.3 Dependency of J_c on the field angle. 9
2.4 Experimental setup. 11
2.5 Experimental setup 12
2.6 Experiment instrumentation. 12
2.7 Schematic view of the voltage taps location. 13
2.8 Coil critical current. 15
2.9 coil critical current. 15
2.10 Coil self-inductance. 16
2.11 Profile of the current profile injected in the coil. 17
2.12 Comparison between the measured magnetic field at the bore and the applied current. 18
2.13 Comparison between the measured potential difference at the bore and the applied current. 19

3.1 Geometry of the 2D axial-symmetric simulation in COMSOL. . . . 23
3.2 Detail of the tape in the geometry implemented in the simulation. . 24
3.3 Zoomed view of the mesh in the tape. 26
3.4 Mesh of the total simulated domain. 26
3.5 J_c as a function of the magnetic field. 28
3.6 Magnetic field variation in time for different values of RRR of the coil supports. 29
3.7 Potential difference at 4 K during the RRR measurment. 31
3.8 Uncertainty determination results. 34
3.9 Magnetic field 300 A. 35
3.10 Potential difference 300 A. 36
3.11 Dissipated energy 300 A. 37
3.12 Magnetic field 400 A 37
3.13 Potential difference 400 A. 38
3.14 Dissipated energy 400 A. 38

3.15 Magnetic field 500 A . . . 39
3.16 Potential difference 500 A. . . . 39
3.17 Dissipated energy 500 A. . . . 40
3.18 Magnitude of the current induced in the copper supports. . . . 41
3.19 Hysteresis loss per cycle in the three experiments . . . 42
3.20 Eddy currents loss per cycle in the three experiments . . . 42
3.21 Ohmic loss in the copper support per cycle in the three experiments 42

4.1 Magnetic field 300 A (Matlab). . . . 50
4.2 potential difference 300 A (Matlab). . . . 50
4.3 Dissipated energy 300 A (Matlab). . . . 51
4.4 Magnetic field 400 A (Matlab). . . . 52
4.5 Potential difference 400 A (Matlab). . . . 52
4.6 Dissipated energy 400 A (Matlab). . . . 53
4.7 Magnetic field 500 A (Matlab). . . . 53
4.8 Potential difference 500 A (Matlab). . . . 54
4.9 Dissipated energy 500 A (Matlab). . . . 54
4.10 Total magnetic field at the center of the system compared with the field generated only by the coil and by the current induced by each of the copper supports. . . . 55

5.1 Analytical magnetic field distribution. . . . 57
5.2 Analytical expressions. . . . 60

6.1 Schematic representation of a twisted striated HTS tape under varying magnetic field. . . . 62
6.2 AC losses scheme. . . . 65
6.3 Screening currents. . . . 66
6.4 Redistribution of the current in a striated HTS tape when it meets a local defect. . . . 69
6.5 Fishnet pattern. . . . 70
6.6 Brickwall pattern. . . . 70

7.1 2LUPS method. . . . 72
7.2 Critical current experimental setup. . . . 74
7.3 Reference tape critical current. . . . 75
7.4 Striated tape critical current. . . . 76
7.5 Current density distribution reference tape. . . . 78
7.6 Current density distribution in the striated tape ($\rho = 25\rho_{Cu}$). . . . 79
7.7 Current density distribution in the striated tape ($\rho = \rho_{Cu}$). . . . 80
7.8 Current density distribution in the striated tape (L=L_C). . . . 81

Abstract

High-temperature superconductors (HTS) based on REBCO represent a key technology for the realization of high-field magnets in fusion reactors and particle accelerators. However, HTS magnets operated in AC regime generate a significant amount of AC losses, which can lead to thermal instabilities. This master's thesis provides a wide study on this topic. A set of experiments performed on an HTS pancake in AC regime was analyzed and compared to FEM models, as well as to a simple semi-analytical model and to the analytical formulations available in literature. In addition, an analysis of striated HTS tapes is performed, analyzing the conditions in which they are effective in reducing AC losses. The experiments studied were performed on a 67-turn pancake coil wound with a 12 mm tape electrically insulated with StyCast. The experimental campaign was performed at the Paul Scherrer Institute and was originally aimed at testing the cooling ability of a conduction-cooled system based on a two-phase Neon Pulsating Heat Pipe (PHP); all the experiments were performed at 30 K. Initially, some preliminary tests were done to evaluate the critical current (1160 A) and the self-inductance of the coil (0.387 mH); these tests were performed at a low current ramp rate. The actual test campaign consisted of AC cycling experiments with a ramp rate of 150 A/s and a maximum current that varied between 300 A and 500 A. These experiments revealed unexpected electromagnetic behavior: the central magnetic field presented an amplitude reduction and a phase shift, and the voltage deviated from the expected trend. These phenomena highlighted a strong electromagnetic interaction with the surrounding copper components. To better understand the physical phenomena that characterize the experiment, a 2D FEM model was developed in COMSOL Multiphysics. The model coupled the H-formulation, used for the highly non-linear superconductor domains, with the A-formulation, used for the normal conductors and air. A detailed characterization of the copper RRR value was also performed, since it was observed to be one of the most critical properties of the system. A rigorous uncertainty quantification analysis was conducted evaluating the numerical uncertainty introduced by the mesh and the uncertainty introduced by the uncertainty related to the RRR value. The model showed good agreement with the experimental data and gave the possibility to understand where

the losses came from. It proved that more than 80% of the total energy dissipated comes from the currents induced in the conduction-cooling copper supports. In parallel, a lumped-parameter model was implemented in MATLAB. It is based on a system of ordinary differential equations coupled through a mutual inductance term. This model gave a good approximation of the experimental results, even if much less computationally complex than the other one. Finally, the last chapters are dedicated to striated HTS tapes. 3D FEM simulations together with analytical models were used to show in which cases the filamentation process is effective in reducing the losses when subjected to a varying magnetic field. The most significant parameters in reducing the AC losses were identified in the frequency at which the field varies, the transverse resistance between filaments and the length of the sample. A review of the different methods for producing the striation was presented, with particular attention to the innovative Two-Level Undercut-Profile (2LUPS) technique.

Chapter 1

Introduction

High-Temperature Superconductors (HTS), and specifically second-generation Rare-Earth Barium Copper Oxide (REBCO) coated conductors, have emerged as the foundational technology for next-generation magnets. The great advantage of this conductors is their ability to sustain high critical current densities under intense background magnetic fields and operate at temperatures significantly above those required by conventional Low-Temperature Superconductors (LTS), REBCO tapes provide viable pathways toward future fusion reactor and next-generation particle accelerators.

Despite these outstanding intrinsic properties, practical implementation under transient and alternating operating regimes remains challenging. Standard coated conductors possess an extreme aspect ratio, the superconducting layer with a thickness of only a few micrometers (1–3.5 μm) deposited on substrates several millimeters wide. When subjected to time varying magnetic fields these planar geometries experience substantial alternating current (AC) losses, this effect is particularly strong when the magnetic field is perpendicular to the wider face of the tape. These losses are primary due to the hysteresis in the superconducting layer and eddy currents induced in the layer of normal conducting metal in the tape (copper stabilizer, Hastelloy substrate, silver cap). In cryogenic environments, such dissipation generates a continuous thermal load that can compromise thermal stability and lead to quench if the heat is not properly removed.

Furthermore, in conduction-cooled superconducting magnets, to guarantee thermal and mechanical stability bulky structural supports made of copper are often used. Because copper exhibits very low electrical resistivity at cryogenic temperatures, time-varying magnetic flux generates strong induced currents within these supports. These eddy currents produce significant magnetic shielding that can distort the field in the bore and generate a large amount of Joule heating that can largely surpass the losses of the coil itself.

1.1 Goal of the Thesis

This work addresses the electromagnetic behavior and loss mechanisms of HTS conductors from two complementary perspectives:

1. **Electromagnetic Analysis of an HTS Coil in Transient Regimes:** Investigating experimentally and numerically the electromagnetic dynamics and AC losses of a 67-turn insulated pancake coil wound with a 12 mm THEVA REBCO coated conductor. This experiment, carried out at the Paul Scherrer Institute (PSI), with the original purpose of determining the cryogenic thermal performance of Neon Pulsating Heat Pipes (PHP) under rapid current variations, is adopted here as an experimental case study to benchmark AC loss models. The primary objective is to evaluate and separate the individual loss contributions, by benchmarking experimental measurements against a Finite Element Method (FEM) model and a lumped-parameter circuit model.

2. **AC Loss Mitigation Strategy via Striated REBCO Tapes:** Evaluating conductor filamentation as a strategy to mitigate magnetization hysteresis losses. This is performed through the numerical analysis of the 12-filaments tape manufactured by Subra and by comparing these results with standard non-striated tapes.

1.2 Structure of the Thesis

The thesis is organized as follows:

- **Chapter 2: Case Study – Experiment Description** details the experimental setup of the 67-turn HTS pancake coil cooled by Neon PHPs. It reports preliminary characterization measurements, including critical current determination and self-inductance evaluation, followed by the presentation of experimental data (magnetic field, coil voltage, and cycle energy dissipation) during cyclical current ramps.

- **Chapter 3: Computational FEM Simulation** presents the 2D axisymmetric numerical model developed in COMSOL Multiphysics, which combines the H-formulation in the superconducting tape with the A-formulation in the copper supports and surrounding domains. It details the RRR characterization of the copper supports, provides a rigorous numerical grid convergence index (GCI) and input uncertainty evaluation, and analyzes the breakdown of dissipated energy.

- **Chapter 4: Analytical Simulations** introduces a semi-analytical lumped-parameter model implemented in MATLAB. The system is represented as

three resistive circuits (coil, upper support, and lower support) inductively coupled and solved using ordinary differential equations (ODEs) to predict transient voltages, bore fields, and losses.

- **Chapter 5: Analytical Formulations for AC Losses** discusses semi-analytical methods for determining the radial profile of the magnetic field across the winding pack and compares the simulated hysteresis losses against classical analytical models for superconducting strips and slabs (Kajikawa model).
- **Chapter 6: Possible Strategy for AC Losses Mitigation: Striated Tapes** provides a theoretical framework for conductor striation, describing individual loss mechanisms (hysteresis, eddy currents, and inter-filament coupling), deriving the critical coupling length L_c.
- **Chapter 7: Case Study: Subra HTS Striated Tape** investigates the 12-filament 2LUPS coated conductor by Subra. It details the multi-step fabrication procedure, presents experimental critical current measurements at 77 K comparing the striated tape with a reference tape, and discusses 3D numerical simulations (H-ϕ formulation) evaluating the impact of inter-filament transverse resistance and tape length on filament decoupling.

Chapter 2

Case study - Experiment description

To obtain experimental data for studying the behavior of HTS under time-varying current, a set of experiments performed on a HTS insulated pancake coil was analyzed. This set of experiments was done to test the ability of Pulsating Heat Pipes (PHP) to properly cool a coil in realistic working conditions. PHP is a device that passively transfer heat using the oscillating motion of a two-phase fluid, without any pump. It consists in a capillary tube bent into many turns; the fluid evaporates in the hot section and condenses in the cold region. In this case the heat source is the heat produced by the coil and the cold region is kept at constant temperature since is connected to a cryocooler. The experiments were performed in such a way that the current was continuously fast ramped in the coil generating a significant amount of AC losses the had to be exhausted via the PHP. Neon was used as a cooling fluid in the PHP, the working pressure was 0.98 bar, so the working temperature of the cooling fluid was 27 K that is the condensation temperature for Neon at the considered pressure. The working temperature of the fluid in a PHP only depends on the fluid and the working pressure since it must work in two phases (liquid and gaseous) to properly transmit the heat; so, the temperature will always be the condensation temperature of the fluid. For this reason all the experiments were performed in this temperature condition. This set of experiments even if it was not properly designed to analyse AC losses in HTS coils gave an important set of data to benchmark the analysis.

2.1 Coil geometry description

2.1.1 Pancake parameters

The coil used in this experiment is a 67 turns pancake coil wound with a 12 mm ReBCO coated conductor tape manufactured by THEVA. The coil was electrically insulated using a StyCast paste with alumina particles in it. The StyCast was chosen as an insulator because it can guarantee good insulation at low temperatures. The alumina particles were added to the StyCast paste to guarantee a physical separation between the tapes, to achieve this goal the alumina particles must be around the 15% of the StyCast weight. In this case the average size of the alumina particles was 32×10^{-6} m. The inner diameter of the coil is 60 mm, and the outer diameter is 86 mm, considering that the tape thickness is 150×10^{-6} m the average insulation thickness between the tapes is 50×10^{-6} m. This value is slightly higher than the average alumina particle size, this happens because there can be also particles bigger than the average size and because two or more particles can be one behind the other so that the effective thickness of the insulating layer increases. The average thickness of the insulating layer was evaluated using the following formula:

$$d_{\text{ins}} = \frac{r_{\text{out}} - r_{\text{in}} - N_{\text{turns}} \cdot d_{\text{tape}}}{N_{\text{turns}}} = 0.05 \text{ mm} \tag{2.1}$$

The HTS tape is soldered to copper supports from which the current is injected in the coil. The tape soldered to the copper is a 'double tape' with this expression it is indicated two tapes soldered together. This process is done because the current injection and the soldering of the tape to the copper supports are considered risky areas and dangerous operations, by adding a second tape the critical current of the coil in that area is doubled and the risk of having a damage there is reduced. In the table below are reported some significant dimensions of the coil.

Parameter	Value
Tape width	12 mm
Inner diameter	60 mm
Outer diameter	86 mm
Total tape length	15.85 m
Tape thickness	150 μm
Insulating thickness	50 μm

Table 2.1: Main geometrical parameters of the coil



Figure 2.1: Upper view of the pancake coil

2.1.2 Tape description

The tape used is a 12 mm THEVA TPL 4000. As all ReBCO coated conductors it is formed of many different layers. The tape is surrounded by a 20 μm copper coating, then there is a 100 μm of Hastelloy sub layer, 3.5 μm of MgO, 3.5 μm of GdBaCuO (superconductive layer) and a 1.5 μm silver layer [1]. the Hastelloy is mainly composed of Nickel, Chromium and Molybdenum with lower content of Iron and Tungsten [2].

Layer	Thickness
Copper surrounding	20 μm
Silver layer	1.5 μm
GdBaCuO (superconducting layer)	3.5 μm
MgO layer	3.5 μm
Hastelloy layer	100 μm

Table 2.2: Layer architecture and dimensions of the THEVA TPL 4000 coated conductor.

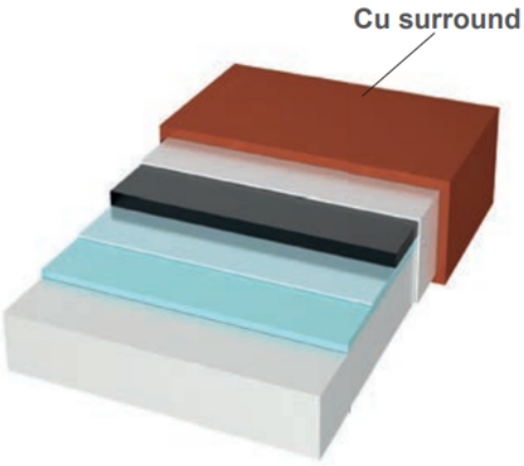


Figure 2.2: Schematic view of a generic coated HTS conductor.

Unlike other superconductor manufacturers, THEVA does not deposit the HTS layer perpendicularly to the substrate but with an angle around 30°, this happens because they use the Inclined-Substrate Deposition method.

This changes the critical current dependence on the angle. In fact, usually the highest performance in terms of critical current is achieved when the applied field if parallel to the tape width and the worst performance are achieved when the magnetic field is perpendicular to the tape, in THEVA tape these angles are shifted of 30°.

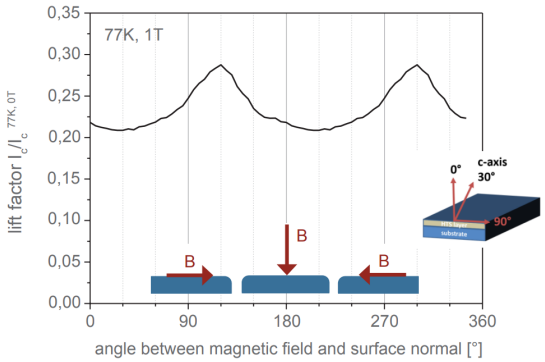


Figure 2.3: The graph show the dependency between the angular between applied magnetic field and the tape and the lift factor at $77K$ and $1T$

The tilted HTS layer gives some advantages compared to the standard procedure. In fact, in this case not all the HTS grains have the same orientation, so the anisotropy is slightly reduced [3], in addition the Inclined-Substrate Deposition

allows the growth of thicker HTS layer without introducing major defects, allowing the critical current per unit width to increase significantly [4].

2.1.3 Coil supports

The coil is surrounded by copper supports that serve several functions:

- inject the current from the power supply into the coil;
- provide mechanical support, preventing deformation due to the strong Lorentz forces that arise at high current;
- ensure thermal coupling between the coil and the PHP, allowing efficient heat transfer;
- maintain a uniform temperature throughout the coil.

The current is injected in the copper plates through two L-shaped copper pieces that are then connected to the power supply. This connection can be seen in figure 2.4. The current then flows into the coil through two circular sections to which the HTS tape is soldered to (figure 2.1). Since the current must cross some copper and a joint to be injected into the coil, there will be some Joule heating due the resistance of the copper. However, the losses in this area will be limited since the resistivity of the copper is very low and the cross section in which the current flows is always very large. In any case, these losses are evaluated with properly placed voltage taps.

During the experiments the coil was subjected to AC current, this means that also the generated field varies in time. Consequently, the Lorentz's force to which the coil is subjected varies significantly. The current in the coil flows always in the same direction, and so the Lorentz force generated is also always directed radially towards the outside of the coil. This force, if the pancake is not properly protected, can cause vibrations of the tape that can ruin it or locally heat it, causing a local variation of its properties. For this reason, the coil must be properly impregnated and the support must be sufficiently solid. To make the system more stable, a layer of StyCast is put between one copper plate and the coil, to guarantee that the contact between the coil and the supports. To avoid any movement, it is important that the supports have a coefficient of thermal expansion (CTE) close to the one of the HTS tape. This is particularly important in the joint area where stress concentration could potentially ruin the tape, in this experiment this problem is not present since the supports are in copper which is the same material that coats the tape. In the final experimental set up, two additional copper plates were clamped to the coil supports (this can be seen in 2.4). The PHPs are put inside these plates. Figure 2.5 is show half of these plates, another half covers the rest of the PHP. Each

of the two plates, assembled as described, are clamped to the coil support (figure 2.4) in this way the PHP is in thermal contact with the coil and can exhaust the heat that it generates. To properly exhaust the heat and to guarantee a proper thermal contact is fundamental that the thermal conductivity of the coil supports and of the PHP supports is sufficiently high, for this reason both parts are made in high purity copper. The high thermal conductivity of copper for the supports has also the advantage of guaranteeing that the temperature can be considered constant all over the coil, guaranteeing the same properties in all the points. It also guarantees that the heat is exhausted fast.

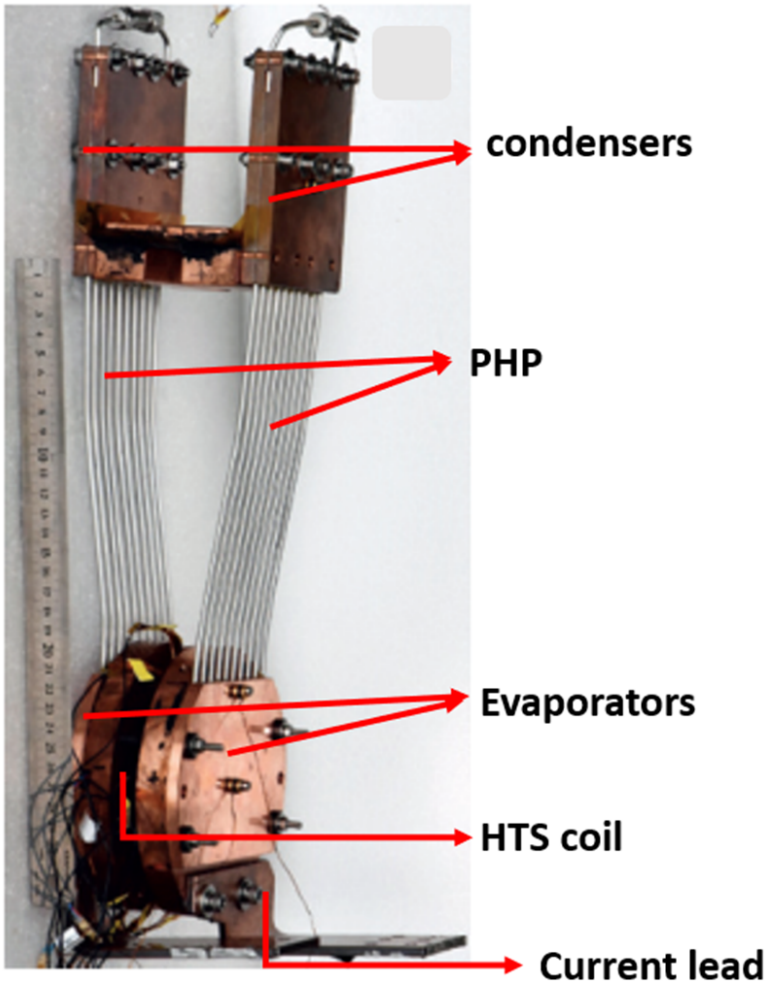


Figure 2.4: Experimental setup.

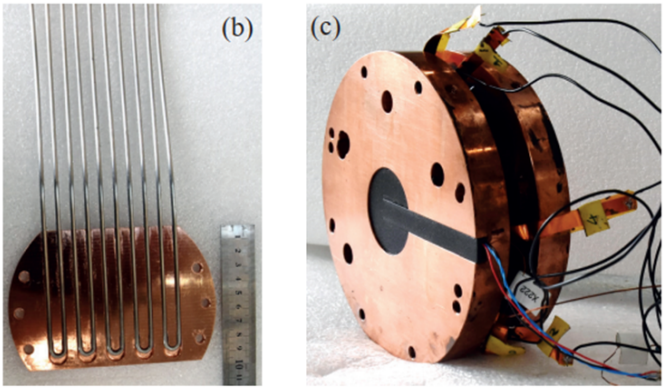


Figure 2.5: Experimental setup

2.1.4 Instrumentation

The whole system requires many sensors and different kinds of instruments to properly run the experiment and to properly acquire the desired data. The instrumentation used in the experiment is schematized in the figure 2.6:

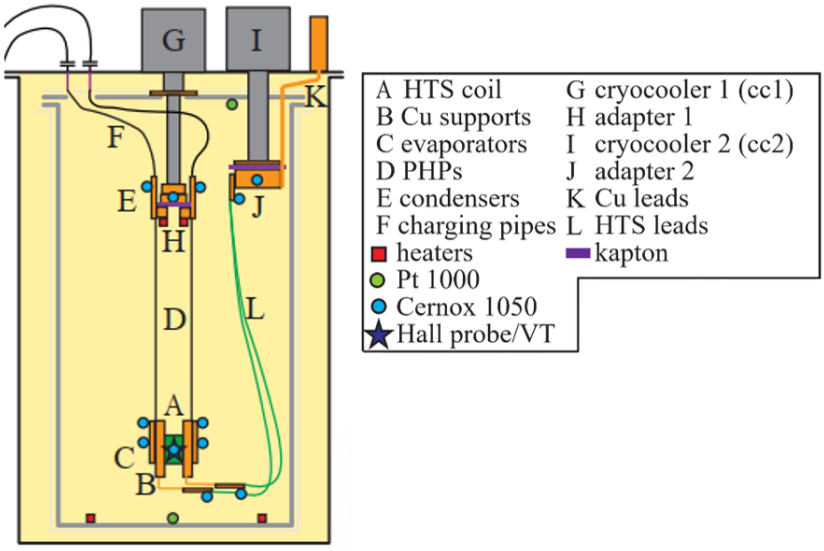


Figure 2.6: Scheme of the position of the instrumentation used in the experiment.

- **Four heaters**: two are installed on each side of the condenser, while the other two are located on the radiation shield. The first pair is used to control the condenser temperature, ensuring that it remains stable at the condensation

temperature of neon through a Proportional-Integral-Derivative (PID) control system.

- **Twelve Cernox 1050 temperature sensors**: one is placed inside the coil near the first turn, while the others are distributed on the condensers, evaporators, and HTS current leads. These sensors operate in the temperature range between K and 290 K, with an accuracy of $\pm 10 - 40\ mK$.

- **Two PT1000 temperature sensors**: these are mounted on the radiation shield, one on the lower part and one on the upper part. They operate in the temperature range between 70 K and 290 K, with an accuracy of $\pm 0.3\ K$.

- **One TOSHIBA THS119 Hall sensor**: it is positioned at the center of the coil to measure the generated magnetic field.

Other than these sensors, 8 voltage taps were placed along the coil to monitor the voltage difference across the coil. The voltage taps are visible in figure 2.1, each voltage tap was coated with an additional tape to ensure additional protection and to ensure electrical insulation from the rest of the coil.

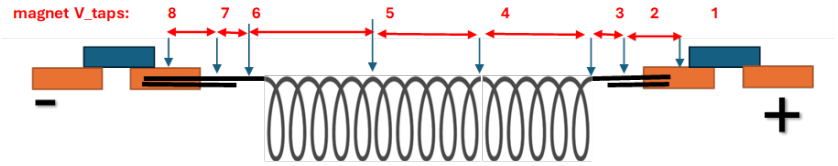


Figure 2.7: Schematic view of the voltage taps location.

- **Voltage taps 1 and 8** are located in the current injection region, where the HTS tape is soldered to the copper supports.

- **Voltage taps 2 and 3, and 6 and 7** are positioned immediately after the current injection at the first turn and just before the injection at the last turn. In each pair, the taps are placed close to each other to provide redundancy, as this signal is critical for the quench protection of the coil.

- **Voltage taps 4 and 5** are placed after 23 and 44 turns, respectively. This configuration divides the coil into three sections, allowing the location of a quench to be identified.

The signals from the eight voltage taps and the Hall sensor are recorded using the Universal Quench Detection System (UQDS).

2.2 Preliminary analysis

Before starting with the actual experiment, it was necessary to run some preliminary tests to prove that the coil works properly and to quantify some important quantities that characterize the coil.

2.2.1 Critical current

The critical current of the coil was measured by slowing increasing the current until the protection system was activated. The test was run increasing the current with a low ramp rate to reduce the inductive voltage and to eliminate the possible phenomena that can occur when the current is ramped fast. To have a more solid result the experiment was done twice, the first time with a current ramp rate of 2 A/s and the second one with a current ramp rate of 10 A/s. Both cases gave very similar results, so only the first case will be analyzed from now on. To evaluate the critical current, the potential difference between the current terminals was divided by the total conductor length (15.85 m) to get the electric field. At this point, this result was used to fit the power law formula.

$$E = E_0 \left(\frac{I}{I_c} \right)^n$$

The value of E_0 is set equal to 0.1 mV/m, as is standard for high-temperature superconductors. The experimental results of the electric field are used to determine the best fit for I_c and the n-value using nonlinear least-squares minimization. The resulting fitting curve is shown in figure 2.8. The results of the fitting are n-value equal to 12 and critical current equal to 1161 A.

As it is shown in the plot the experimental data never reached the E_0 value but it was stopped before, this often happens in large magnets, because being the total length of the used tape large, the total potential difference can be large and potentially ruin the coil even if the electrical field generated is still far from the E_0 value. For this reason in this case there is not a direct intersection between the experimental data and the critical electric field but the critical current was evaluated considering the fitting curve and its intersection with the critical electric field.

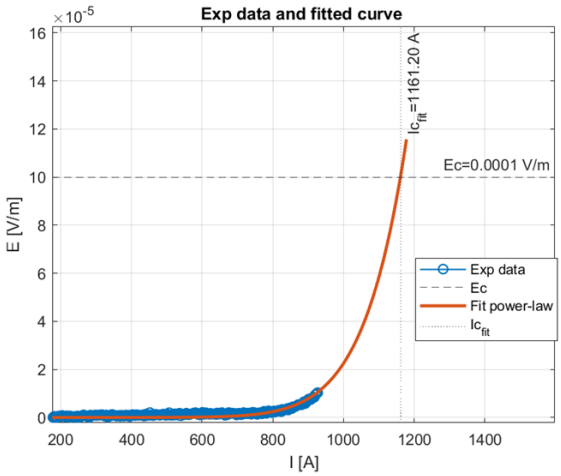


Figure 2.8: Experimental data from the critical current experiment and the best fit these data using the power law.

In figure 2.9 the potential difference of each section of the coil are shown. According to the voltage taps numeration the 'section 3-4' is the internal one, the 'section 4-5' is the intermediate and the 'section 5-6' is the outer one. The plot shows that the section that experienced the highest increase in potential difference is the innermost section, this happened because it is the section that is subjected to the highest magnetic field, and since the critical current density strongly depends on the magnetic field the area with the highest field is the one that reaches the critical current first. The fact that this clearly happens in the coil also is one proof that there are no major defects that induce a quench at lower current.

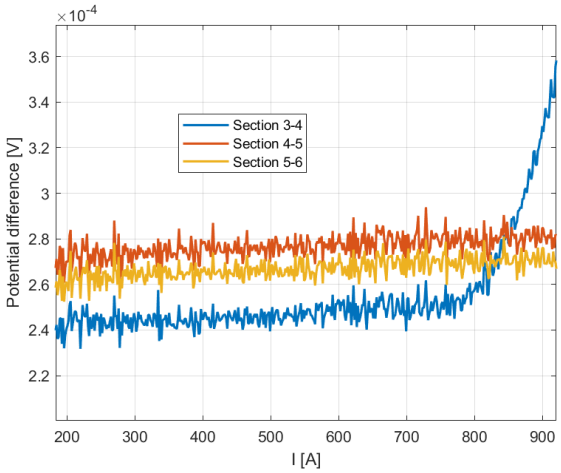


Figure 2.9: Potential difference in each of the three section of the coil.

2.2.2 Inductance

To evaluate the coil inductance, it was run an experiment in which the current starting from 20 A was ramped at 10 A/s until 500 A, once this value was reached the current was maintained constant for some time and then the current was reduced to 20 A with the same ramp rate. This process was repeated twice. To evaluate the inductance, it was used the following formula:

$$U_{\text{ind}} = L\frac{dI}{dt} \tag{2.2}$$

The current profile in time and the corresponding potential difference is shown in the figure 2.10.

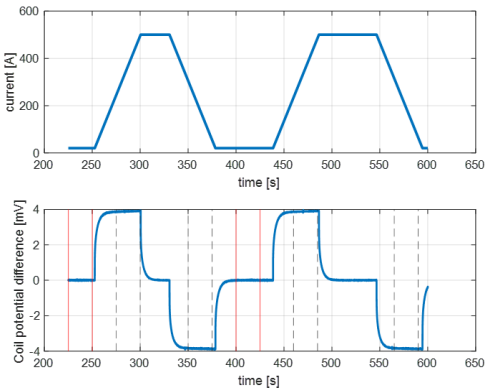


Figure 2.10: Fig.a Shows the time profile of the current in the coil. Fig.b Shows the coil potential difference recorded during the experiment.

It was evaluated the average potential difference, in absolute value, in the areas in between the dashed black lines; it was also evaluated the average potential difference in the intervals between the red lines, in these two latter intervals the potential difference should be null, so this extra procedure was done to evaluate a potential offset in the measurement. Once these values are known, the offset was subtracted to the average potential difference, and the result was divided by the current ramp rate. The result was an inductance of 0.387 mH.

2.3 Experiment

The experiments had the goal to verify the ability of a PHP of cooling an HTS coil that works in AC. To prove this, the experiments had to be sufficiently long to ensure that the system is in stationary conditions and the current injected had to reach such values at such ramp rate to produce significant losses. Many experiments

were conducted in which the maximum current reached was of 100 A, 200 A, 300 A, 400 A and 500 A, the current increased linearly until the maximum current is reached, then it was set a plateau of 0.1 s, at this point the current decreases with the same linear ramp rate until it goes back to 0 A, to close the cycle a plateau of 0.1 s is set also at $0A$. The current ramp rate at which the experiments were performed are: 50 A/s, 100 A/s, 150 A/s, 200 A/s and $500A$ $/s$. The rest of the analysis focuses on three experiments all of them with current ramp rate of 150 A/s and with current varying between 0 A and 300 A in the first experiment, 400 A in the second and 500 A in the third experiment. In all experiments at least 100 cycles were performed, to be sure that the steady-state was reached. In the figure below is shown an example of the current profile in time in the case of maximum current equal to 300 A and current ramp rate equal to 150 A/s, with the 0.1 s plateaus at 300 A and 0 A.

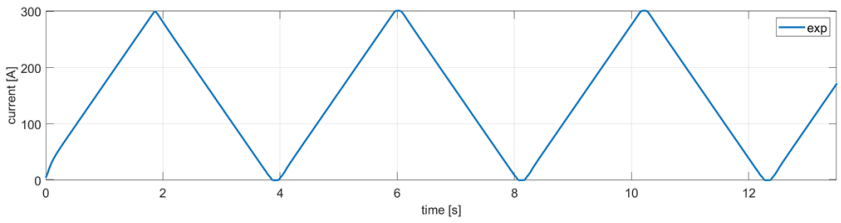


Figure 2.11: Profile of the current profile injected in the coil.

2.4 Results

In this section the results of the experiment with maximum current 500 A will be analyzed in detail. The analysis of the other two experiments will be analyzed in the section 3.4 however, what will be said for this experiment is also valid for the other two.

The analysis will focus on the magnetic field generated, the potential difference between the two extremities of the coil and the energy dissipated per cycle. To plot the results more easily only the first 5 cycles are shown, but as mentioned above, the experiments consist in at least 100 cycles. However, after the first two or three cycles the behavior of each quantity repeats cyclically.

2.4.1 Magnetic field

The magnetic field was evaluated in the center of the coil with a Hall sensor; it was placed at the center of the circumference formed by the coil and half of the width of the tape. In the figures below are presented the plot of the measures of the experiment, the results are presented together with the current profile and the

maximum value of magnetic field that the coil was expected to generate at the maximum current, this value is represented by the black dashed line denoted as 'B Biot' in the legend.

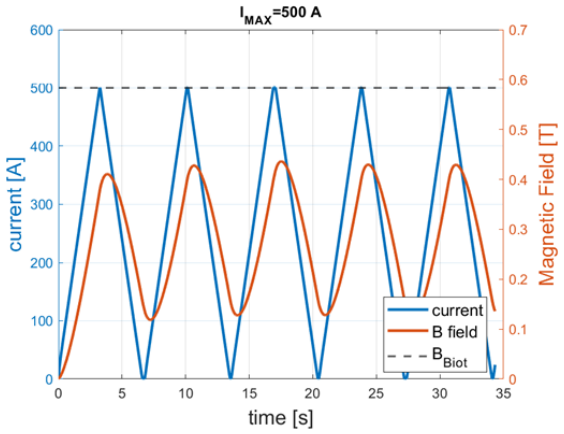


Figure 2.12: Comparison between the measured magnetic field at the bore and the applied current ramp ($I_{\max} = 500$ A, $\mathrm{d}I/\mathrm{d}t = 150$ A/s).

The value 'B Biot' is evaluated using the following approach:

- The magnetic field is evaluated using the Biot-Savart law by considering the contribution of each turn when the maximum current flows in the coil. The turns are assumed to be equally spaced between the inner and outer radii.

$$B_n = \frac{\mu_0 I_{\max}}{2r_n} \tag{2.3}$$

- The total magnetic field at the center of the coil is obtained by summing the contributions of all turns:

$$B_{\text{tot}} = \sum_{n=1}^{N} B_n \tag{2.4}$$

- The radius of an equivalent coil is then calculated as:

$$R_{\text{eq}} = \frac{\mu_0 N I_{\max}}{2B_{\text{tot}}} \tag{2.5}$$

What is found following this procedure is the radius of an equivalent coil in which all the current that flows in the real one flows in a circumference of radius

R_{eq}. The result that was obtained is $R_{eq} = 36.1mm$ that is slightly different from the average coil radius that is $R_{ave} = 36.5mm$.

In the experiment there are some unexpected characteristics: the magnetic field never reaches the maximum value expected, after the first instant the magnetic field never returns to be null, the magnetic field is not proportional to the current but is lower than expected when the current is increasing and higher than expected when the current is decreasing, the peak value reached in the first cycle is slightly lower than the one that is reached in the other cycles. All these facts cannot simply be a consequence of the uncertainty related to the sensor or of the sensor being misplaced. As it is going to be proof, in the following sections and chapters, these unexpected events are due to the strong currents induced in the copper supports.

2.4.2 Potential difference

The potential difference across the coil is recorded with the UQDS system. The results are shown in figure2.13 in the same way used to present the data for the magnetic field.

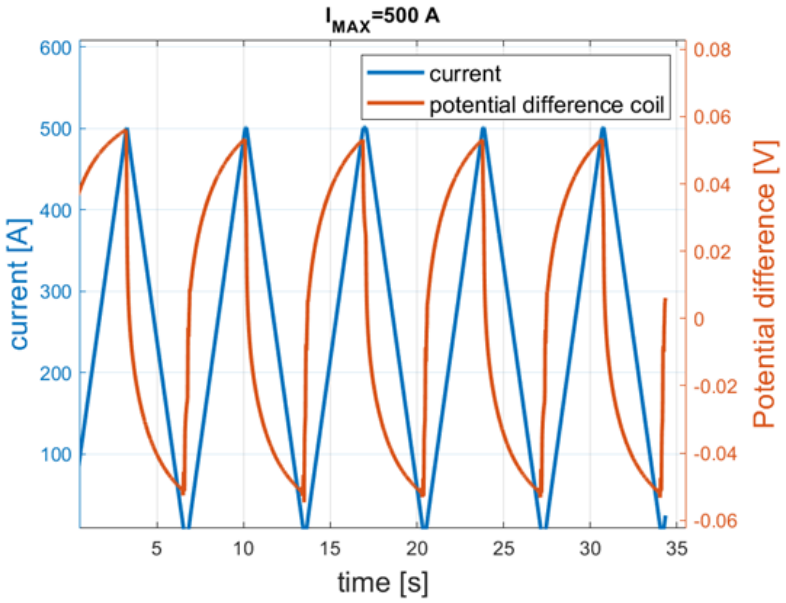


Figure 2.13: In the picture the behavior of the potential difference in time (red line) is compared to the applied current (blue line).

Also for this quantity the expected results do not match what was found experimentally. The expected behavior was that the potential difference would be mainly due to the coil inductance, so a profile close to what appeared in the

inductance evaluation: a square wave with amplitude equal to

$$U_{ind} = L_{coil}\frac{dI}{dt} = \pm 0.058V \tag{2.6}$$

However, the experiment showed a profile far from a square wave, the signal oscillates between values that are in absolute value smaller than the expected ones and the peak value reached in the first cycle is slightly higher than the one reached in the rest of the experiment. Again, this will be explained in the following chapters considering the current induced in the copper supports.

2.4.3 Energy dissipated

To evaluate the power dissipated it is used the method presented in [5], it will be called 'electric method'. The method consists of integrate over a period the product of current and potential difference.

$$E_{\text{cycle}} = \int_{t_0}^{t_0+t_{\text{cycle}}} I\,\Delta V_{\text{coil}}\,dt \tag{2.7}$$

With this method is possible to evaluate the average energy dissipated in one cycle and can be used only when the system is in steady state. Using this equation, it is not possible to determine the instantaneous dissipated power, because the product of the current and the voltage difference represents the total instantaneous power, which includes both the dissipative contribution and the term associated with the variation of magnetic energy stored in the system due to inductive effects. The latter contribution is positive when the current in the coil is increasing, as energy is being stored in the magnetic field, and negative when the current is decreasing, as the magnetic field releases energy back to the electrical circuit. However, the stored power integrated over one cycle when the system is steady is always null, so integrating over a period the dissipated energy is the only contribution left.

$$E_{\text{cycle}} = \int_{t_0}^{t_0+t_{\text{cycle}}} P_{\text{losses}}\,dt + \int_{t_0}^{t_0+t_{\text{cycle}}} P_{\text{stored}}\,dt \tag{2.8}$$

$$\int_{t_0}^{t_0+t_{\text{cycle}}} P_{\text{stored}}\,dt = 0J \tag{2.9}$$

It is important to highlight that the result obtained in this way is the average energy dissipated in the whole system not just in the coil. In fact, even if in the formula it is consider the current flowing in the coil and the difference of electrical potential at the extremities of the coil, the coil is magnetically connected to the copper supports: the magnetic field produced by the current in the coil induces currents in the supports. The system can be described as three electrical circuits

(the coil, and the two supports) that mutually exchange magnetic energy with each other but only one of these circuits (the coil) is connected to the power supply. Intuitively, if only one circuit is connected to the power supply all the energy stored and dissipated in the system must come from the power supply. In the table below are reported the average energy dissipated in each analyzed experiment, the value reports the energy dissipated in the 10^{th} cycle.

$I_{\max}$	Energy dissipated
300 A	5.08 J
400 A	9.52 J
500 A	14.55 J

Table 2.3: Energy dissipated per cycle for different maximum currents

Chapter 3

Computational FEM simulation

To achieve a comprehensive understanding of the physical phenomena occurring during the experiment, a numerical simulation based on the Finite Element Method (FEM) using the software COMSOL Multiphysics was implemented. The simulation results enabled a quantitative evaluation of the phenomena that characterize the experiment. For example, it was possible to separate the total energy lost in three different contributions: resistive losses on the supports, hysteresis losses, eddy-currents losses in the copper coating of the tape. The simulations are done considering exclusively the electrical and magnetic variables, neglecting any temperature variation. This assumption was made because looking at the experimental data it was seen that the maximum temperature variation is around 0.5 K. Such a variation has a negligible influence on the critical current and on all the physical properties of the experiment. The temperature is considered fixed at the value of 30.

3.1 Simulation setup

3.1.1 Simulation geometry

The experimental setup was simulated with a 2D axial-symmetric model.

The pancake coil is modeled with a series of rectangles; more specifically, each turn of the coil is formed of two rectangles that represent the copper coating of the tape, one rectangle that represents the HTS layer, one rectangle that represents the remaining part of the tape (silver, MgO and hast-alloy layers) the properties that are associated with the latter rectangle are weighted on the thickness of each layer, the last rectangle in each turn represent the StyCast insulating layer. In the

table below are summarized the thickness of each layer used in the simulation. The width of all the rectangles is equal to the width of the tape, 12 mm.

Layer	Thickness
Copper surrounding	20 μm
GdBaCuO (superconducting layer)	3.5 μm
Homogenized layer	105 μm
Insulating layer	50 μm

Table 3.1: Thickness of each tape layer in the COMSOL simulation

Other than the actual pancake it is important to properly simulate the supports of the coil and of the PHP since they are strongly magnetically coupled with the coil. Four supports are present in the simulation, each of them is represented as a rectangle: two are the PHP supports and have dimension 72.5×7 mm and the other two are the coil support with dimension 72.5×16.7 mm. Since the simulation is a 2D axial-symmetric the supports could not be represented completely. The main approximation that were made are: considering the PHP supports as completely made of copper, neglecting the steel tubes in them; neglecting the two semicircular areas used to inject the current clearly visible in figure 2.1. The distance between the upper support and the coil is 2.5 mm while the bottom support is only 0.5 mm apart from the coil. All around the system is placed a semicircular area of air with a radius of 0.5 m.

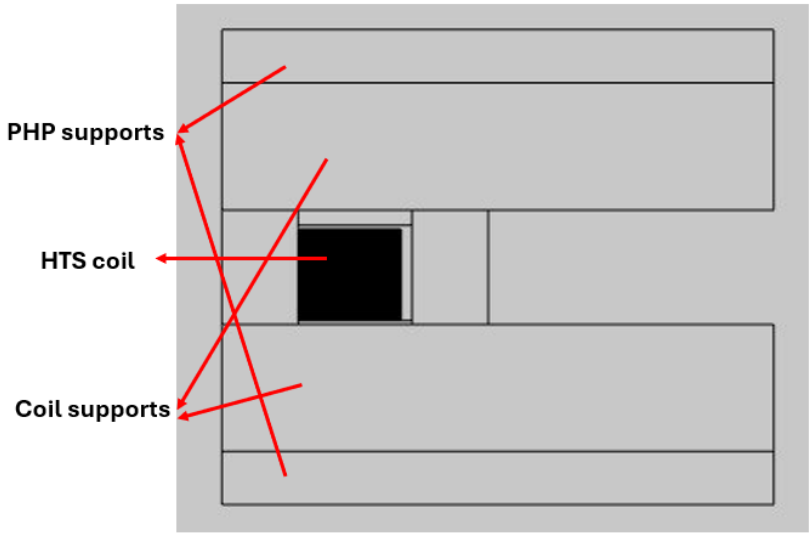


Figure 3.1: Geometry of the 2D axial-symmetric simulation in COMSOL.

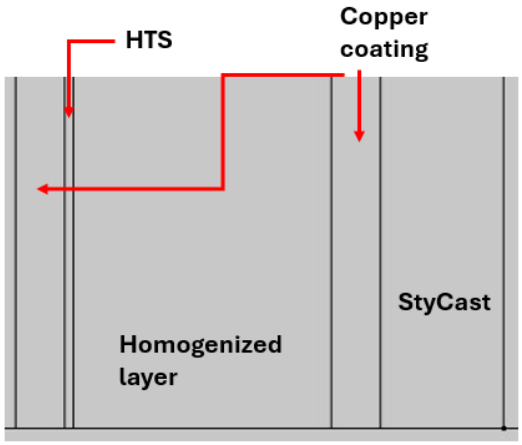


Figure 3.2: Detail of the tape in the geometry implemented in the simulation.

3.1.2 Models

Two models were used in the simulations. The H-formulation is used for the simulation of the tape and the A-formulation for the simulation of all the rest of the domain: air, copper supports, StyCast insulation.

The H-formulation is present in COMSOL as Magnetic Field Formulation (fmh). This formulation gives a precise distribution of the current density and of the magnetic field starting from the Ampere's law, the Faraday's law and the constitutive equation that gives the relation between the electric field and the current distribution:

$$\nabla \times \mathbf{H} = \mathbf{J} \tag{3.1}$$

$$\nabla \times \mathbf{E} = -\mu \frac{\partial \mathbf{H}}{\partial t} \tag{3.2}$$

$$\mathbf{E} = \rho(\mathbf{J})\mathbf{J} \tag{3.3}$$

Substituting the Ampere's law in the constitutive law the following result is obtained:

$$\mathbf{E} = \rho(\nabla \times \mathbf{H})\,(\nabla \times \mathbf{H}) \tag{3.4}$$

Now inserting this result in the Faraday's law, the final result is [6] [7]:

$$\nabla \times [\rho(\nabla \times \mathbf{H})\,(\nabla \times \mathbf{H})] = -\mu \frac{\partial \mathbf{H}}{\partial t} \tag{3.5}$$

This is a partial differential equation that is function only of H. This form allows the equation to be solved also when the relation between the electrical field and the current is strongly non linear as in the superconductors [6]. This formulation is used in the HTS tape because can deal with the non linearity of the superconductors and because it evaluates directly the current. But, compared to the A - formulation, is more computationally expensive so it is not implemented in the whole domain. In the A-formulation (found as fm in COMSOL) is based on the definition of a magnetic vector potential A, defined as:

$$\mathbf{B} = \nabla \times \mathbf{A} \tag{3.6}$$

This can be done since the magnetic field is solenoidal and such fields can always be written as the curl of another field.

Substituting this definition and the constitutive law of the conductors in the Faraday's and Ampere's law the result is:

$$\nabla \times \left(\mu^{-1} \nabla \times \mathbf{A}\right) + \sigma \frac{\partial \mathbf{A}}{\partial t} + \sigma \nabla V = \mathbf{J}_s \tag{3.7}$$

where J_s is the current source, σ is the electrical conductivity, and V is the electrical scalar potential. This formulation is particularly used for modeling the magnetic field and induced current distribution area around coils [8]. The main advantage of this formulation is that the Gauss' law for the magnetic field is automatically satisfied; in addition, in the 2D axisymmetric geometries the A field must be solved only in the z-direction so it has only one unknown instead of the two of the two present in the H-formulation. However, the A-formulation does not solve directly for the magnetic field, but to get to the magnetic field the scalar potential must be derived; in addition this formulation can be highly unstable in case of strongly non-linear conductors with very high electrical conductivity such as superconductors.

3.1.3 Mesh

The domain of the simulation was meshed in an appropriate way to manage to capture all the relevant physical phenomena.

Each layer of the tape (copper coating, HTS, homogenized layer) and the StyCast insulation were meshed using the mapped meshed method imposing only one element on the horizontal direction and 150 elements in the vertical direction. With these numbers the mesh is fine enough to properly capture the complex current density distribution in the HTS layer maintaining an adequate aspect ratio. Figure 3.3 shows a detailed view of the mesh within a tape.

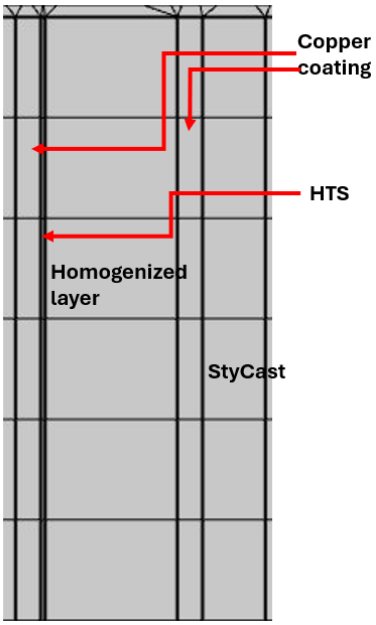


Figure 3.3: Zoomed view of the mesh in the tape.

Also the copper supports are meshed with the mapped method to guarantee an appropriate number of elements in an area where the current density induced is very relevant for the experiment. The remaining domain is meshed with a triangular mesh using the automatic COMSOL values.

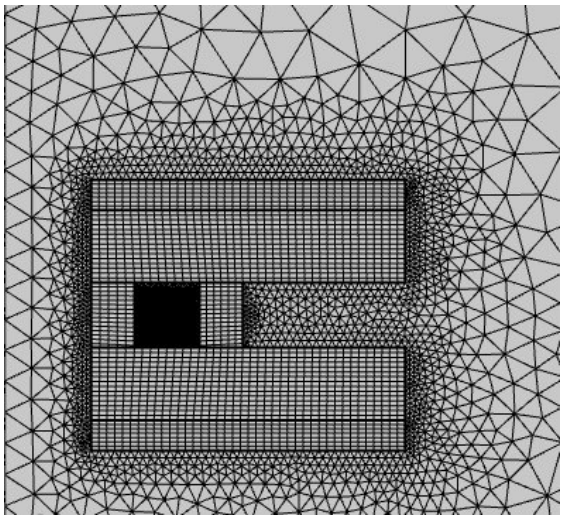


Figure 3.4: Mesh of the total simulated domain.

3.2 Simulation parameters

Once the geometry and the mesh are set the most important parameters to be implemented are the critical current of the superconducting tape and the electrical resistivity of each material.

3.2.1 Critical current

The critical current is important because is used to model the electrical resistivity of the HTS layer using the power law:

$$\rho = \frac{E_c}{J_c(B)} \left(\frac{J}{J_c(B)} \right)^n \tag{3.8}$$

this parameter influences, in particular, the voltage and the losses across the HTS layer. The critical current of the coil was found experimentally and it is equal to 1162 A. however, since the magnetic field varies significantly across a wide range of values to have a more realistic formulation it is important to use a critical current that is a function of the magnetic field. The dependency between magnetic field and the critical current was found on the dataset of the Victoria University of Wellington [9], that is a dataset where the critical current of many different HTS tapes are evaluated experimentally at different temperature, magnetic field magnitude and magnetic field angle. In this case the data considered are the critical current of the THEVA Pro-Line Advanced Pinning 2G HTS in function of the magnitude of the magnetic field keeping the temperature constant (30 K) and the angle between tape and magnetic field (0°); regarding the temperature, any temperature variation can be neglected during the experiment since the experimental data indicates no significant variation in temperature. This temperature is the mean temperature indicated by the temperature sensor placed close to the coil; naturally, is slightly higher than the $27K$ at which the cooling fluid is kept. Considering the angle between the magnetic field and the tape always constant is a much stronger assumption but it can be done considering that on most of the coil the angle is actually close to 0° and because the value for the null angle is an intermediate value among those available.

The data from the Victoria University Dataset had to be scaled on the experimental critical current. This procedure was done following these steps:

- a simulation was run with constant electrical resistivity and current reaching the experimental coil critical current.
- It was evaluated the average of the magnetic field norm on the innermost HTS layer. This value is assumed to be the value of magnetic field that causes the coil to quench, in this case this value is 2.45 T.

- It is evaluated the ratio between the ratio between the experimental critical current and the value indicated in the University of Victoria database when the tape is subjected to 2.45 T.
- All the values of critical current at different magnetic field of the database are multiplied times the ratio found in the previous point.

The final relation between critical current and magnetic field is shown in figure 3.5.

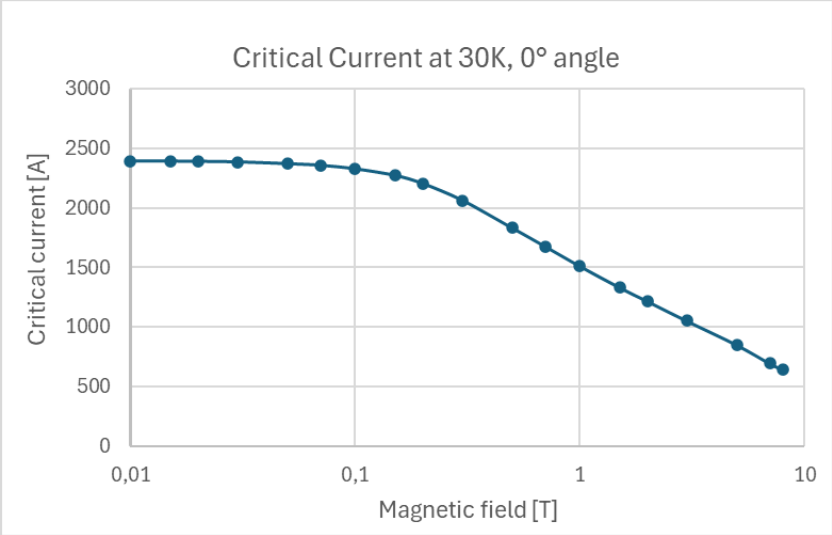


Figure 3.5: Relationship between Critical current and magnetic field of the 12 mm THEVA tape, at 30K with the magnetic field parallel to the tape. These data are the ones implemented in the COMSOL simulation.

3.2.2 Electrical resistivity

The last parameter that had to be set to properly perform the simulations is the electrical resistivity of the other materials present in the experiment. The resistivity of the Sty-Cast and of the air domain was set equal to 1 Ωm, even though the actual value of both the material should be higher, this value is often used to model the non-conductive area around the coil [10]. It provides a sufficiently large value avoiding the flow of current in those areas but it does not increase too much the computational time. The electrical resistivity of the homogenized layer is evaluated by weighting the electrical resistivity of each sub-layer based on its thickness.

$$\rho_{\text{hom}} = \left(\frac{s_{\text{Ag}}}{\rho_{\text{Ag}}} + \frac{s_{\text{Hs}}}{\rho_{\text{Hs}}} + \frac{s_{\text{Mg0}}}{\rho_{\text{Mg0}}} \right)^{-1} \quad s_{\text{hom}} = 5.76 \times 10^{-8}\,\Omega\,\text{m} \tag{3.9}$$

The value of electrical resistivity of the various material were found in [11] and [12].

It was observed that the electrical resistivity of the copper has a very strong effect on the final results. This happens because the experiment is strongly influenced by the currents induced in the copper supports, the magnitude of these currents are directly proportional to the variation of magnetic field flux and inversely proportional to the electrical resistivity of the copper. In the figure 3.6 it is shown an example of this strong influence, the magnetic field in the center of the coil is shown in the graph, the current ramp rate is 500 A/s up to a maximum current of 500 A. The simulation was done with a set of different RRR value and also in the case without any support around the coil.

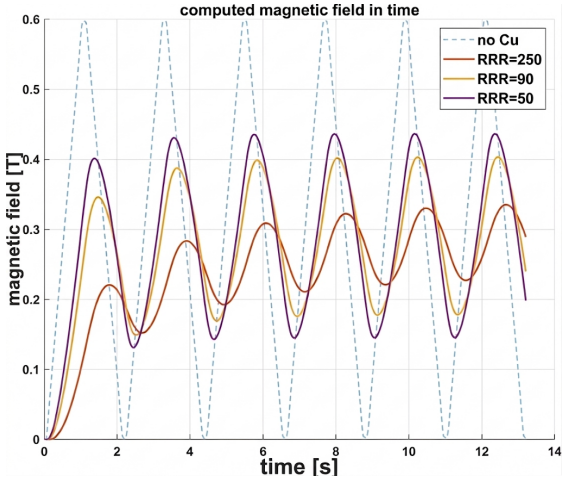


Figure 3.6: Magnetic field variation in time for different values of RRR of the coil supports.

The graph results can be explained as follow: the current induced in the supports tends to oppose to the variation of magnetic field, for low values of resistivity the magnitude of this current is higher, so the effect of the magnetic field will differ a lot from the one in which the there are no supports; vice versa if the resistivity is higher, the current induced are of lower magnitude and the magnetic field will tend to the case without the supports. it was done a set RRR measurement on two copper sample made of the same copper of the supports to establish the exact value if copper resistivity to impose in the simulation. This experiment is discussed in detail in the next section.

3.2.3 RRR measurement

The Residual Resistance Ratio (RRR) is a measurement defined as the ratio between the electrical resistivity of a material at room temperature and its electrical resistivity at 0 K.

$$RRR = \frac{\rho_{300K}}{\rho_{0K}} \tag{3.10}$$

Of course this is just a theoretical formulation, in practical case the denominator is evaluated at 4. This value indicates the level of purity of a material, a high level of RRR indicates a low concentration of impurity and crystal lattice defects. Two strips of the same copper used for the supports were taken to perform the experiment. The two strips were both 9 cm long but they have different cross section: one is 5×2 mm and the other 2×2 mm. The cross section of the strips have to be sufficiently small to induce a detectable voltage across the sample. Two different strips were measured for redundancy; however, both yielded almost identical results. Consequently, all the data reported in this section refer to the 2×2 mm sample.

The experiment is performed imposing a constant current of 1 A and constantly reducing the temperature from room temperature down to 4 K. They were glued to a thick copper block that with its high thermal capacity assured that the temperature variation was sufficiently slow and homogeneous in time. The strips were glues with a thin layer of electrically insulating material to prevent electrical contact between the strips and the block.

When the temperature of 4 K was reached, the cool-down was stopped and the direction of the current was reversed; in this way a possible offset in the data acquisition system can be considered and canceled, the same procedure was done at the temperature of 10 K, 20 K and 30 K. In the figure 3.7 the result of the potential difference at 4 K while reverting the current direction are shown. By dividing this value by the current flowing in the sample and by an appropriate geometrical factor that considers the length and the cross-section of the sample the resistivity of the copper at 4 K is found.

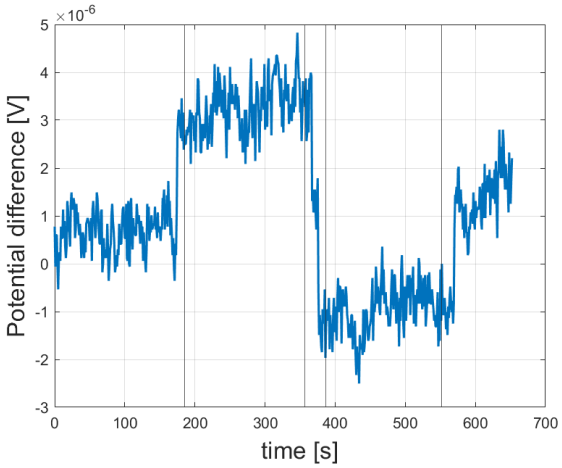


Figure 3.7: Potential difference across the 2×2 mm strip at 4. The plot shows the potential difference before and after the inversion of the polarity.

The result given with the related error is: $\rho_{4K} = (2.29 \pm 0.02) * 10^{-10}\ \Omega \times m$

The error is a consequence of the oscillation of the voltage present during the experiment. The same procedure is done for the resistance at room temperature obtaining: $\rho_{300K} = 1.81 \times 10^{-8}\Omega \times m$. In this case the value is given without a corresponding error because the number of values collected in this case is so high that the error is several orders of magnitude lower than the average value.

With these data the resulting RRR is: $RRR = \ 78.9 \pm 0.3$. The electrical resistivity was evaluated using the correlation in [13] that relates the electrical resistivity with the RRR and the temperature. With this result the value of resistivity for copper used in the simulations is $\rho_{Cu}(T = 30K) = (2.803 \pm 0.008) \times 10^{-10}\Omega \times m$.

3.3 Uncertainty quantification

To evaluate the quality of the simulations and of their result it was performed an uncertainty quantification analysis. It was evaluated the numerical uncertainty and the uncertainty related to the RRR value. Both the uncertainty are evaluated in the case with maximum current equal to $500A$.

3.3.1 Numerical uncertainty

The numerical uncertainty was evaluated performing three simulations with different meshes. One simulation was the original one with the mesh presented in the subsection 3.1.3; the second one is coarser than the first one with half of the element on the width of the tape (75 instead of 150) and with approximately half

of the element on the coil and PHP supports; the third mesh is finer than the reference one with double the elements on the tape width (300 instead of 150) and approximately double the elements on the copper supports. The number of elements on each layer of the tape remained constant and equal to one. With these characteristics the ratio between the number of elements in the first mesh and the second one and between the second one and the third one is similar and almost equal to 2. From this moment the finer mesh will be called mesh 1, the intermediate mesh as mesh 2 and the coarser mesh as mesh 3. The numerical uncertainty is measured using the total energy lost per cycle as a reference value. The procedure followed to achieve this result is the five step method presented in [14]:

1. For each mesh is defined a representative mesh size h.

$$h = \sqrt{\frac{\sum_{i=1}^{N} \Delta A_i}{N}} \tag{3.11}$$

2. Once the three meshes are defined, it must be calculated the grid refinement ratio. It is the ratio between the h values of two consecutive meshes.

$$r = h_{coarse}/h_{fine} \tag{3.12}$$

   According to [14] this ratio must always be larger than 1.3.

3. The apparent order of convergence is evaluated solving the following system of non-linear equation.

$$\epsilon_{21} = E_2 - E_1 \tag{3.13}$$

$$\epsilon_{32} = E_3 - E_2 \tag{3.14}$$

$$s = sign(\frac{\epsilon_{32}}{\epsilon_{21}}) \tag{3.15}$$

$$q(p) = \ln \frac{r_{21}^p - s}{r_{32}^p - s} \tag{3.16}$$

$$p = \frac{1}{\ln r_{21}}(\ln |\frac{\epsilon_{32}}{\epsilon_{21}}| + q(p)) \tag{3.17}$$

   The system can be solved starting from $q(p) = 0$.

4. At this point the extrapolated value for the energy dissipated per cycle can be calculated:

$$E_{ext} = \frac{r_{21}^{p} E_1 - E_2}{r_{21}^{p} - 1} \tag{3.18}$$

   This value is the value that would be obtained with a mesh with representative mesh size $h \to 0$.

5. Finally the Grid Convergence Index (GCI) and the numerical uncertainty (u_{num}).

$$GCI = \frac{F_s |E_1 - E_2|}{r_{21}^{p} - 1} \tag{3.19}$$

$$u_{num} = \frac{GCI}{k} \tag{3.20}$$

   The recommended value for k and F_s is for a conservative estimate on an unstructured grid refinement are 1.1 and 3 respectively.

Table 3.2 reports the numerical values obtained by the procedure presented above.

r_{21}	1.41
r_{32}	1.41
E_1	$13.927J$
E_2	$13.933J$
E_3	$13.945J$
E_{ext}	$13.922J$
p	2.11
GCI	0.12%
u_{num}	0.11%

Table 3.2

It can be highlighted how the values of dissipated energy for the three simulations are monotonically decreasing towards the value extrapolated from the 5 step procedure, this is evident in the bar plot 3.8.

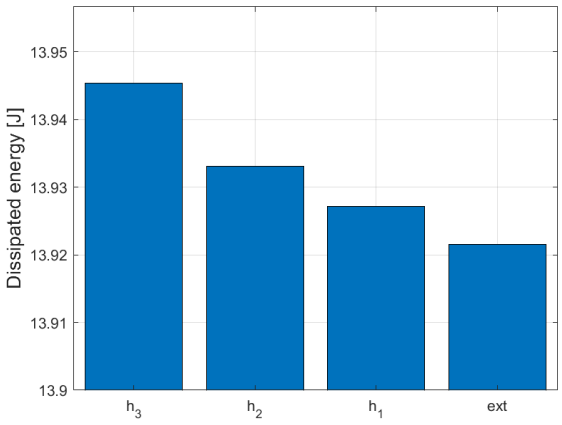


Figure 3.8: Total energy dissipated per cycle according to the three simulations and the extrapolated value resulting from the numerical uncertainty procedure.

3.3.2 Input data uncertainty

To further investigate the crucial role that is played from the resistivity of the copper, it is analyzed the uncertainty related to the RRR measurement.

According to what is obtained in section 3.2.3, the electrical resistivity in the copper is $\rho_{Cu} = (2.803 \pm 0.008) \times 10^{-10} \Omega m$. To evaluate the uncertainty introduced from this value two additional simulations were performed, one with the upper value of ρ_{Cu} and another one with the lower value. With these two simulations it is possible to evaluate the sensitivity coefficient of the total energy dissipated for the electrical resistivity:

$$\frac{\partial E}{\partial \rho_{Cu}} = \frac{Q(\rho_{Cu} + \Delta\rho_{Cu}, ...) - Q(\rho_{Cu} - \Delta\rho_{Cu}, ...)}{2\Delta\rho_{Cu}} + O(\Delta\rho_{Cu}) \tag{3.21}$$

This formula allows the evaluation of the influence of ρ_{Cu} on the total energy dissipated per cycle. By multiplying this result times the uncertainty related to ρ_{Cu} the uncertainty of the dissipated energy related to ρ_{Cu} is obtained.

$$u_{input} = \frac{\partial E}{\partial \rho_{Cu}} u_{\rho_{Cu}} \tag{3.22}$$

The value obtained is 0.002 J. It means that the uncertainty on this value of input introduces an error of around 0.01%. Performing this analysis on the RRR or directly on the resistivity of the copper gives exactly the same results since they are two quantity that are closely related.

This procedure could be repeated for all the input values to determine the contribution of each value to the final error. However, for lack of the uncertainty values on the other parameters and to simplify the analysis the other input parameters are considered as exact values.

3.4 Results

In this section the results obtained in the simulations are presented and compared to the experimental values. In each of the following subsection the results for magnetic field, potential difference and energy dissipated per cycle for each of the three experiments are presented.

3.4.1 Maximum current 300 A

In figure 3.9 it is shown the magnetic field measured in the center of the of the coil and the magnetic field evaluated in the same position in the COMSOL simulation, the dotted line in the plot represents the maximum value of magnetic field expected from the coil without any inductive effects from the copper supports. The two curves qualitatively have the same behavior and also the numerical values are very close between each other, however, some significant difference must be highlighted. The maximum of the simulated values are always slightly lower than the measured values and the same behavior is observed for the minimum values. Another difference is that in the first part of the cycle, when the current is increasing the simulated magnetic field is always lower than the measured one, while the opposite behavior is observed in the second part of the cycle.

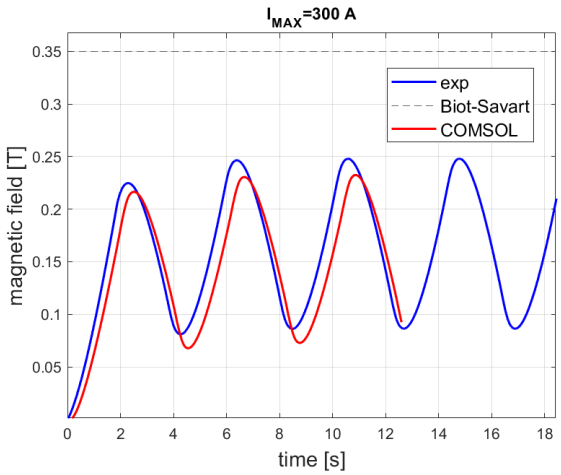


Figure 3.9: Comparison between the magnetic field experimentally measured and simulated in COMSOL in the case with $300A$ of maximum current.

Figure 3.10 shows the comparison between the potential difference of the coil and the simulated one. This last value is obtained by multiplying the average electrical field on the tape times by the length of the tape used in the coil. The

differences between the simulation and the experiment are quite similar to the ones observed in the magnetic field: the simulation underestimates the potential difference in the first part of the cycle and overestimates it in the second one. in addition to this difference, every time that the current derivative in time changes the simulated potential difference has a small spike. This is most probably due to numerical effect due to the strong nonlinearity of the problem.

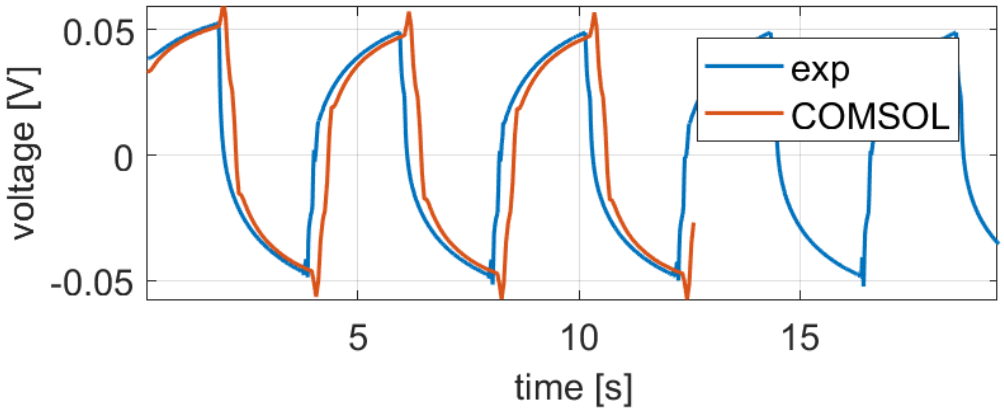


Figure 3.10: Comparison between the potential difference experimentally measured and simulated in COMSOL in the case with $300A$ of maximum current

Figure 3.11 show a bar plot in which the total energy lost per cycle evaluated experimentally is compered whit the total energy lost according to the simulation. A primary advantages of this simulations approach is the ability to separate the total loss into individual contribution. In particular, three contributions where evaluated: the energy dissipated in the HTS layer, the energy lost in the rest of the tape and the energy dissipated from the eddy currents in the copper supports. The last phenomenon is the one contributing the most to the global losses. Globally the losses evaluated experimentally are of $5.089J$ while the numerical model gives a result equal to $5.132 \pm 0.006J$. The uncertainty is due to the phenomena described in the previous section. The two values are quite close to each other, however the experimental value does not fall in the range predicted by the simulation.

3.4.2 Maximum current 400 A

Figure 3.12 shows the comparison between the experimental value of the magnetic field and the magnetic field obtained from the simulation, also in this case,the two lines show a good qualitative agreement. However, in this case the differences between the experimental and simulated magnetic field are different from the previous case, the two curves are basically coincident for most of the cycle but the maximum reached in the simulation are higher than the maximum reached in the

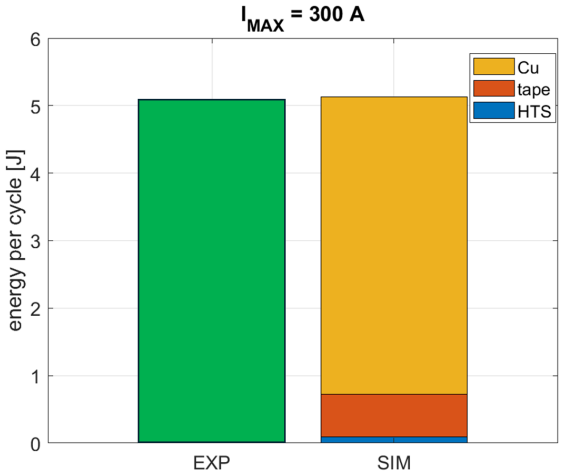


Figure 3.11: Comparison between the energy dissipated per cycle measured experimentally and simulated in COMSOL in the case with $300A$ of maximum current. With the simulation is also possible to divide the losses in different contribution: Cu refers to the losses in the copper supports, *tape* refers to the losses due to eddy-currents in the copper coating of the tape and HTS refers to the hysteresis losses in the HTS layer.

experiment, while the minimum of the simulation are lower than the minimum of the experiment.

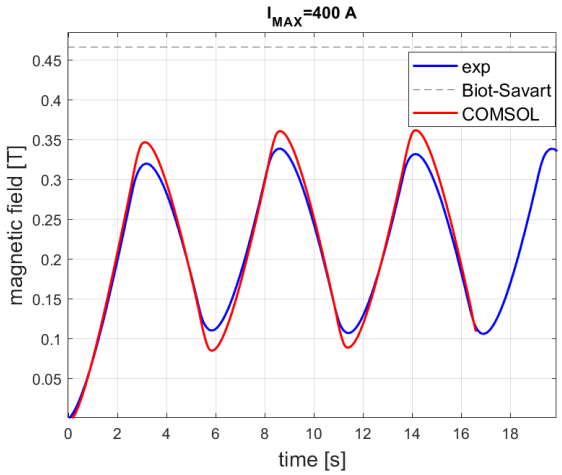


Figure 3.12: Comparison between magnetic field experimentally measured and the one obtained with the COMSOL simulation in the case with maximum current equal to $400A$.

The comparison of the potential difference (figure 3.13), shows that the two profile are very close to each other, again the major difference is the spikes in the simulated profile when the current derivative changes.

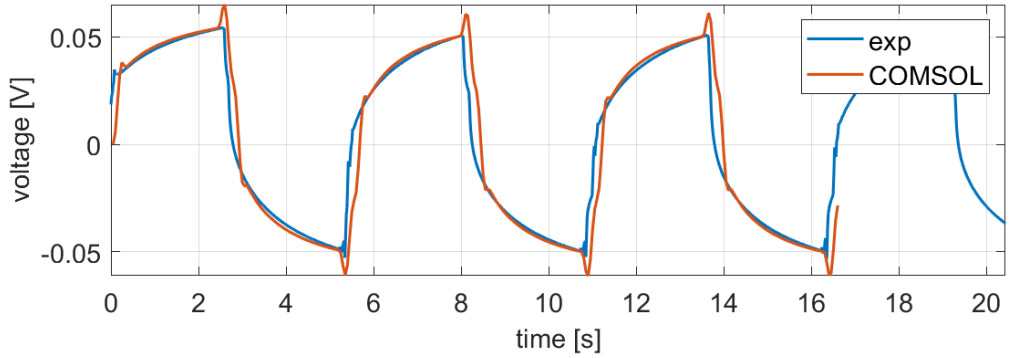


Figure 3.13: Comparison between potential difference experimentally measured and the one obtained with the COMSOL simulation in the case with maximum current equal to $400A$.

In the analysis of the losses (figure 3.14) it appears that the major contribution comes again from the Joule losses in the supports and the relative weight of each of the three contribution is similar to the previous case. However, the experimental value of the energy lost per cycle is $9.517J$ while the value predicted by the simulation is $9.035 \pm 0.011J$, showing a greater deviation with respect with the first experiment analyzed.

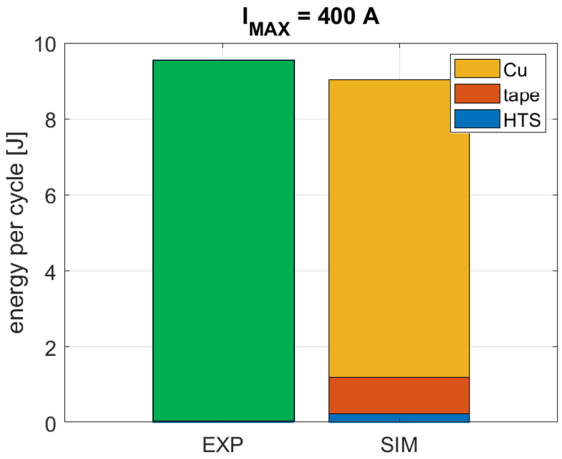


Figure 3.14: Comparison between the energy dissipated per cycle experimentally measured and the one obtained with the COMSOL simulation in the case with maximum current equal to $400A$.

3.4.3 Maximum current 500 A

In the case of third and last experiment (with maximum current of $500A$) what was written for the second one holds true, since the behavior of the three quantities is qualitatively the same and also the differences between what was measured experimentally and what was simulated numerically are the same. For what regards the energy losses the experimental evaluation is equal to $14.548J$ while the numerical model gives a value equal to $13.93 \pm 0.02J$. Also this time the experimental value does not fall in the range predicted by the COMSOL simulation.

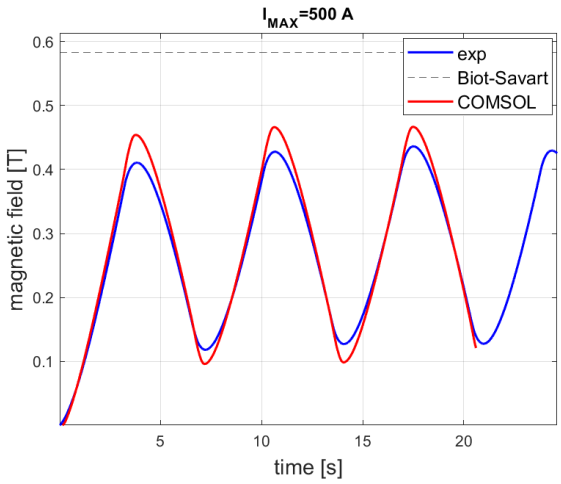


Figure 3.15: Comparison between magnetic field experimentally measured and the one obtained with the COMSOL simulation in the case with maximum current equal to $500A$.

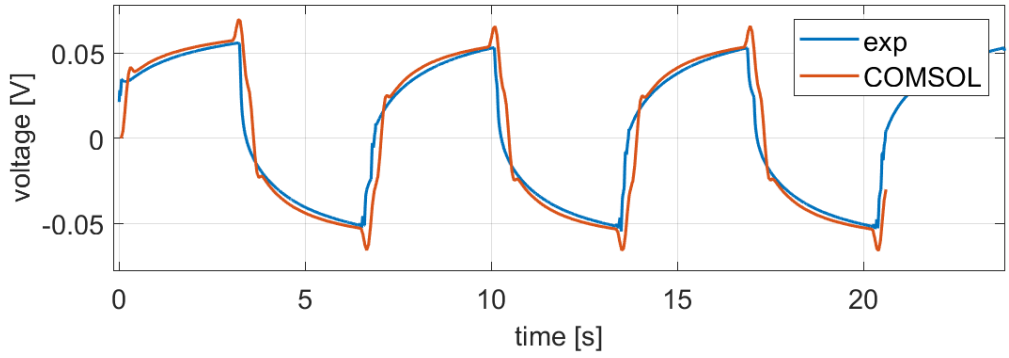


Figure 3.16: Comparison between the potential difference experimentally measured and the one obtained with the COMSOL simulation in the case with maximum current equal to $500A$.

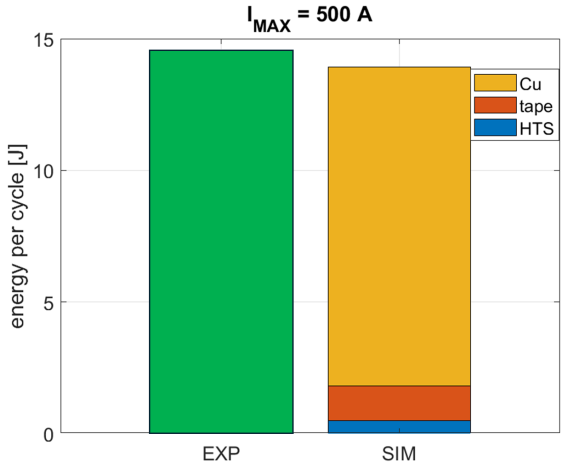


Figure 3.17: Comparison between energy loss per cycle experimentally measured and the one obtained with the COMSOL simulation in the case with maximum current equal to $500A$.

To further validate the hypotheses that the behavior of the magnetic field is due to the current induced in the copper supports it is reported in figure 3.18 the sum of all the current induced in each support in the experiment with maximum current equal to $500A$ according to the COMSOL simulation. From the plot the first thing to be noticed is the order of magnitude of the overall current, the maximum of these currents is in the order of 10^4A that is comparable with the maximum current flowing in the coil. This can explain the significant reduction in the maximum value of the magnetic field with respect to the case without copper supports. It also important to highlight the sign of those currents, it shows that direction of this current is such that reduces the variation of magnetic flux: the current is negative when the current in the coil is increasing and so the magnetic flux increasing and vice-versa. Finally, it shows that magnitude of the current induced in the first cycle is slightly higher than the one of the other two cycles, this happens because the starting point of the first cycle is having zero magnetic field, so the variation of the magnetic field in the first cycle is higher than in the others; this difference also explains why the maximum of the magnetic field of the first cycle is slightly lower than in the rest of the experiment as appear in figure 3.15.

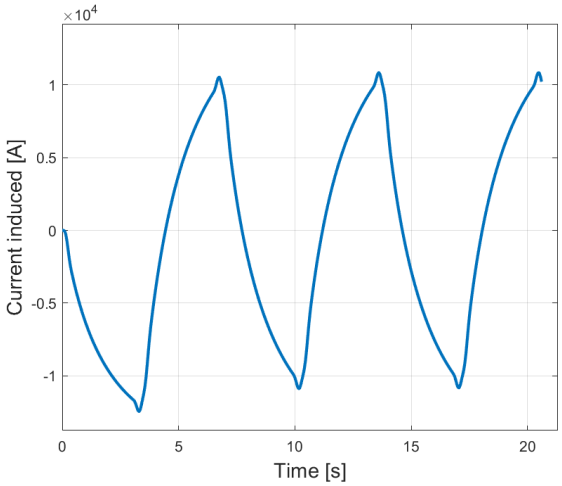


Figure 3.18: Magnitude of the current induced in the copper supports.

Many other discrepancies between the numerical result and the experiment are due to the inevitable differences between the real geometry and the simulated one. In fact, in the simulation being two dimensional and axial-symmetric, the two copper semicircles from which the current is injected into the coil cannot be simulated (figure 2.1). In particular, the inner semicircle is the part of the support subjected to the strongest variation in magnetic field flux, so the highest currents are induced in that area; however, covering only half of the support it cannot be properly represented in the simulation. Other discrepancies between the experiment and the simulation are all the holes, screws and other mechanical parts and the holes left for the PHP, all these factors introduce a difference between the global amount and distribution of the copper, this can change the magnitude of the induced currents and their path. The last important difference introduced in the model is that COMSOL considers the two pairs of coil and PHP support as only one object, while the reality is that are two different bodies clamped together so there is certainly a contact electrical resistivity between the two support that is completely neglected in the simulations.

The only way to properly reproduce all these phenomena is to actually perform 3D simulations considering every geometrical detail. However, the computational effort to perform such kind of simulations is much greater than the one needed to run two dimensional simulations and the quality of the results would not change significantly.

Finally, in figures 3.19, 3.20 and 3.21 the losses in the HTS layer, in the copper coating and in the copper supports in each experiment are reported.

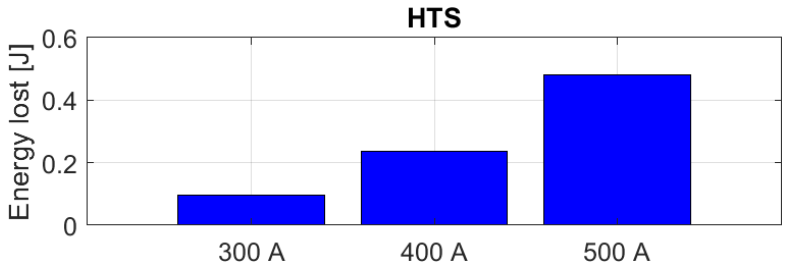


Figure 3.19: Hysteresis loss per cycle in the three experiments

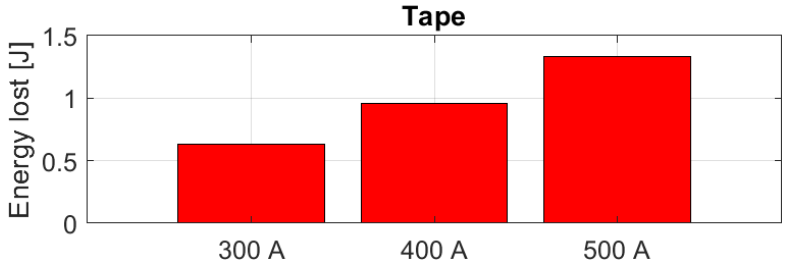


Figure 3.20: Eddy currents loss per cycle in the three experiments

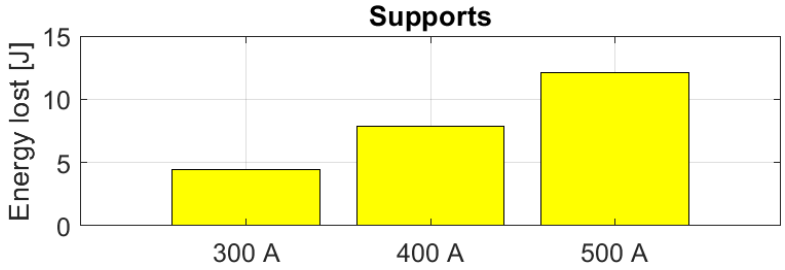


Figure 3.21: Ohmic loss in the copper support per cycle in the three experiments

Those graphs shows again that in each experiment the vast majority of the losses comes from the Joule losses in the copper supports and they show how each category varies with the variation of the current. The highest relative increase between different experiments is in the losses in the HTS layer, this is due to the strong nonlinearity of the power law used to model the resistivity in the superconductor layer. The losses in the copper supports are proportional to the square of the current induced in the supports. It is interesting to notice that the ratio between the losses in the supports in the $400A$ experiment and in the $300A$ one is equal to 1.78, this exact value is found evaluating $(\frac{400}{300})^2$, the same occurs evaluating this ratio between the $500A$ and the $400A$ experiments. This means that this kind of losses is proportional to the square of the peak current flowing in the coil.

The results of these experiments prove that in conduction cooled AC magnets the way of exhausting the heat must be carefully optimized to avoid a huge source of heat. One possibility proposed in [15] is to insert some cuts in the supports, in this way the support surface in contact with the magnet remains almost the same meaning that the cooling will not be significantly affected by the cuts but the electrical resistance will increase a lot reducing the current induced and the losses. The electrical resistance will reduce a lot because it depends on the cross section through which the current flows, so if the cuts are deep enough it can be reduced significantly.

Chapter 4

Analytical simulations

The same experiment was studied also through the implementation of a semi-analytical model using MATLAB. This model considers the experimental setup as a set of electrical circuits with condensed parameters and solves the set of equations for the current of each circuit, knowing the current in each circuit it is possible to retrieve the magnetic field in the center, the potential difference at the extremities of the coil and have an estimate of the global losses.

4.1 Equations

The idea in this model is to consider the coil, the copper supports above the coil and the copper supports below the coil as three electrical circuits electro-magnetically coupled between each other. In this model the PHP supports and the coil supports above the coil are considered as a single object, and the same is done for the supports below the coil. A similar approximation was also done in the COMSOL model, in fact, there was no contact resistance between the two kind of supports. Since this approximation did not alter significantly the results in the COMSOL model it was kept also in this model to limit the number of coupled equation to consider.

The equations governing this phenomenon are the one reported below.

$$\begin{cases} V_1(t) = R_1 i_1(t) + L_1 \dfrac{di_1(t)}{dt} + M_{21} \dfrac{di_2(t)}{dt} + M_{31} \dfrac{di_3(t)}{dt} & \text{Coil} \\ V_2(t) = R_2 i_2(t) + L_2 \dfrac{di_2(t)}{dt} + M_{12} \dfrac{di_1(t)}{dt} + M_{32} \dfrac{di_3(t)}{dt} & \text{Upper copper support} \\ V_3(t) = R_3 i_3(t) + L_3 \dfrac{di_3(t)}{dt} + M_{13} \dfrac{di_1(t)}{dt} + M_{23} \dfrac{di_2(t)}{dt} & \text{Lower copper support} \end{cases}$$

The first equation refers to the coil itself, the equation states that the potential difference applied to the coil is equal to the sum of different contributions: the resistive term, the inductive one and the potential difference induced by the current variation in time in the other two circuits. The same equation with different parameters is valid also for the copper supports above the coil (second equation) and for the copper supports below the coil (third equation). The main differences between the coil equation and the other two equations are that the coil has multiple turns while the two sets of supports are modeled as an electrical circuit with a single turn, another important difference is that while $V_1(t)$ varies in time the values of $V_2(t)$ and $V_3(t)$ are forced to zero in each time instant. This second difference is due to the fact that the current induced in the supports is necessarily a closed loop: they are induced in the azimuthal direction and they close once they complete a loop around the support.

Knowing this last detail the system is composed of three unknowns that are $V_1(t)$, $i_2(t)$ and $i_3(t)$ and three equations therefore it can be solved. The other quantities in the system are known or can be estimated. In particular:

- $i_1(t)$ is known being the current imposed in the coil by the power supply.
- $V_2(t)$ and $V_3(t)$ are always equal to zero since the potential difference of a closed loop of current.
- L_1 is known since it was evaluated experimentally and equal to $0.387mH$(see subsection 2.2.2).
- R_2, R_3 and L_2, L_3 can be evaluated knowing the geometry of the system.
- R_1 can be evaluated in such a way that the losses of this model match what was found in the COMSOL model.

4.2 Parameter determination

4.2.1 Electrical resistance

The electrical resistance R_2 and R_3 can be easily calculated since both the resistivity (section 3.2.3) and the geometry of the supports are known using the formula:

$$R = \rho \frac{L}{A} \tag{4.1}$$

The formula states that the electrical resistivity is proportional to the resistivity and to the length of the path traveled by the current and inversely proportional to the cross section through which it flows. In this case the cross section was simply determined as the product of the width of the supports times their height. The

length L is equal to the circumference that has radius equal to the average radius of the coil. It was used this value, instead of the average radius of the supports, because from the FEM simulation it was seen that the highest current density was induced at the average radius of the coil. Of course not all the induced current flows at this position but it can be considered an average position where the model concentrates all the current. Since the two supports are equal the result is the same for both R_2 and R_3 and it is equal to 37.89 $n\Omega$.

The value of R_1 should consider both the resistance of the HTS layer and the losses due to the eddy currents in the coating of the tape. However, it is impossible to condense the complex non-linear behavior of the superconductor into one single parameter, for this reason the resistivity of the coil is measured starting from the power losses evaluated in the COMSOL simulation. Considering R_1 constant in time and independent of the imposed current and on the magnetic field the resistance can be evaluated as indicated in equation 4.2, the values of Q_{HTS} and Q_{tape} are the values of the losses from the HTS layer and the losses in the tape coating that result from the COMSOL simulation with maximum current equal to 400 A. The 400 A experiment will also be used to evaluate the coefficient of mutual inductance between the different circuits.

$$R_1 = \frac{Q_{HTS} + Q_{tape}}{\int_{t_0}^{t_0+period} I_1^2(t)\, dt} \tag{4.2}$$

Using this approach the value of R_1 results equal to $4.0 \times 10^{-6}\Omega$. This value derives from the 400 A experiment but will be used to model also the other two experiments.

4.2.2 Magnetic inductance

The inductance of the coil is known experimentally $L_1 = 0.387\ mH$ (section 2.2.2). The values of L_2 and L_3 are equal between each other since they only depend on the geometry of the support. They are evaluated using the formula presented in [16].

$$L_{2,3} = \mu_0 R_{ave} \log(\frac{8R_{ave}}{R_{eq}} - 2) \tag{4.3}$$

$$R_{eq} = 0.223(a + b) \tag{4.4}$$

In these formulas R_{ave} is the average radius of the coil and a and b are respectively the width and the height of the supports. It was used R_{ave} equal to the average radius of the coil instead of the average radius of the support for the same reason presented in the previous subsection. The numerical value of $L_{2,3}$ is equal to 29.04 nH this value is much lower than L_1 because the self inductive coefficient

depends on the square of the number of turns and, while the coil has 67 turn, the copper supports are modeled as electrical circuits with only one turn.

4.2.3 Mutual inductance coefficient

The mutual inductance coefficient is the quantity that describes how efficiently a change of the current in one coil induces a change in electromotive force in a coil nearby. This quantity is defined as the ratio between the magnetic flux across the second circuit divided by the current in the primary circuit causing the magnetic field.

The coefficient of mutual inductance can be determined also using the following formula:

$$M = k\sqrt{L_1 L_2} \tag{4.5}$$

It states that the mutual inductance between two coils is equal to the square root of the product of the self inductance of the single coils times the coefficient of coupling k, it is a real number between 0 and 1, where 0 represents the case of completely uncoupled circuits while 1 represents two perfectly coupled circuits. The three k parameters were tuned using the 400 A experiment as well. The method used to tune these parameters is to find iteratively the parameters that result in almost exactly the amount of losses found out experimentally with an uncertainty of 2%. With this method the coefficient of coupling obtained are $k_{12} = 0.63$, $k_{13} = 0.67$, $k_{23} = 0.61$.

4.3 Model solution

In this problem the profile of $i_1(t)$ is known since it is the current imposed in the coil from the power supply, so also $\frac{di_1(t)}{dt}$ can be easily evaluated. This last term is equal to 150 A/s when the current is rising, -150 A/s when it is decreasing and null during the plateaus; this is valid for all the three experiments since the current ramp rate does not change. Knowing these two quantities the problem is greatly simplified. First of all it is possible to use only the second and third equation to solve for $i_2(t)$ and $i_3(t)$, then these values can be inserted in the first equation to find the last unknown, $v_1(t)$. Being the potential $V_2(t)$ and $V_3(t)$ always zero the system composed by the last two equations can be written as:

$$\begin{cases} -M_{12}\dfrac{di_1(t)}{dt} = R_2 i_2(t) + L_2\dfrac{di_2(t)}{dt} + M_{23}\dfrac{di_3(t)}{dt} \\ -M_{13}\dfrac{di_1(t)}{dt} = R_3 i_3(t) + M_{23}\dfrac{di_2(t)}{dt} + L_3\dfrac{di_3(t)}{dt} \end{cases}$$

In matrix form the system can be written as:

$$\begin{bmatrix} L_2 & M_{23} \\ M_{23} & L_3 \end{bmatrix} \begin{bmatrix} \frac{di_2}{dt} \\ \frac{di_3}{dt} \end{bmatrix} + \begin{bmatrix} R_2 & 0 \\ 0 & R_3 \end{bmatrix} \begin{bmatrix} i_2 \\ i_3 \end{bmatrix} = - \begin{bmatrix} M_{12} \\ M_{13} \end{bmatrix} \frac{di_1}{dt}$$

Isolating the terms $\frac{di_2(t)}{dt}$ and $\frac{di_3(t)}{dt}$ the form that is actually solved in the MATLAB program is obtained:

$$\begin{bmatrix} \frac{di_2}{dt} \\ \frac{di_3}{dt} \end{bmatrix} = \begin{bmatrix} L_2 & M_{23} \\ M_{23} & L_3 \end{bmatrix}^{-1} \left[- \begin{bmatrix} R_2 & 0 \\ 0 & R_3 \end{bmatrix} \begin{bmatrix} i_2 \\ i_3 \end{bmatrix} - \begin{bmatrix} M_{12} \\ M_{13} \end{bmatrix} \frac{di_1}{dt} \right]$$

The problem, written in this form, is solved using the MATLAB function 'ode45'. This function needs as input the equation system written in the form presented above, a vector containing the time step on which the solution has to be saved and the initial conditions of the unknowns. The vector of time step has as a starting point the time 0 s and as a end point the end of the 10^{th} cycle, for each cycle the solution is evaluated in 1000 points. The initial condition of both of the unknowns is set to $0A$. The output of the function 'ode45' is a vector on which are contained the time steps on which the solution is evaluated and a table that has one column for each unknown of the system and one row for each time step. 'Ode45' uses the Runge-Kutta method to solve differential equations, evaluating the error making the difference between the solution of fifth and fourth order. The Runge-Kutta method follows the same idea of the Euler's method: starting from a known solution at a given time is possible to evaluate derivative at that time and combining the solution and the derivative it is obtained the solution at the following time step. The main difference between the Euler's method the Runge-Kutta one is that the first method uses only the first order derivative at the beginning of each time step, while the second method evaluates the slope at several intermediate points, providing a more accurate estimate of the solution.

Once the values of $i_2(t)$ and $i_3(t)$ are known they can be substituted in the first equation to find the last unknown, $V_1(t)$.

4.4 Results

In this section the results obtained from this method are compared with the experimental results. As in the previous chapter, the results for the magnetic field in the center of the system, the potential difference of the coil and the energy losses for each of the three experiments are presented. In this model the energy losses

can only be subdivided in energy lost in the supports and energy lost in the coil without differentiating the losses in the HTS and in the tape coating.

The magnetic field at the center of the system has to be evaluated summing the contribution of the three current, this contribution has to be properly weighted considering that the currents flowing in the copper supports are not in the same plane as the coil so an other geometrical factor must be included in the the classical Biot-Savart law. The formula used in this case is the following [17]:

$$B_z(\rho, z) = \frac{\mu_0 I}{2\pi r}\left[K(k) + \frac{R^2 - \rho^2 - z^2}{(R-\rho)^2 + z^2}E(k)\right] \tag{4.6}$$

$$k^2 = \frac{4R\rho}{(R+\rho)^2 + z^2}, \tag{4.7}$$

$$r = \sqrt{(R+\rho)^2 + z^2} \tag{4.8}$$

In these formulae R represents the radius of the spire, ρ the radial position inside in which the magnetic field is evaluated, z the position on the z-axis and E(k) and K(k) are the the complete elliptic integrals of first and second species. For all the circuits the value of ρ was null while the value of z was null in the case of the coil and equal to 1.0 *cm* and 0.8 *cm* for the upper and lower supports respectively. The current imposed in the formula is the one obtained from the model for the copper supports and the total current flowing in the coil for the magnet itself, so the current imposed from the power supply times the number of turns.

To evaluate the instantaneous losses the square of current flowing in each circuit is multiplied times the corresponding resistance.

Finally, the evaluation of the potential difference is obtained by simply solving the model with no further derivation.

4.4.1 Maximum current 300 A

Figure 4.1 shows the comparison between the measured field and the results obtained with the MATLAB model. While the values of the peaks and of the minimum are very close to each other, the simulated field profile seems shifted forward in time. This happens because at least in the very first time steps the magnetic field seems decreasing in time reaching also negative values, this behavior is non-physical since the magnetic field generated from the current induced in the supports reduces the variation of magnetic field in the center of the coil but cannot have an effect so strong that determines negative values of the field. This unexpected behavior is either a numerical artifact given by the model or most probably a sign that the distance between the circuits used in the model in not completely coherent with the coefficient of mutual inductance used.

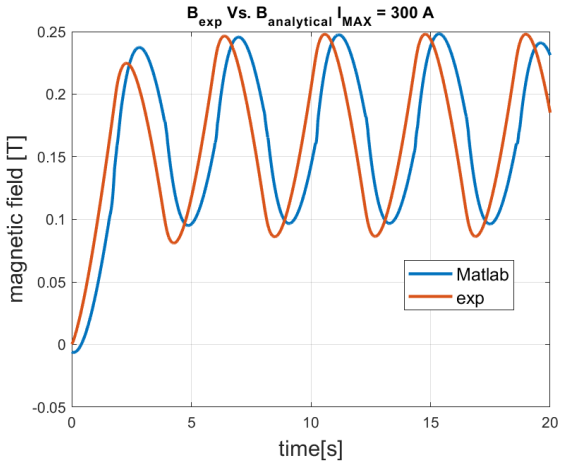


Figure 4.1: Comparison between the experimentally evaluated magnetic field and the magnetic field predicted by the lumped-parameters method in the case with peak current of 300 A.

Figure 4.2 shows the comparison between the potential difference actually measured and the one obtained from the model. The two curves are similar to each other, the peak values are practically the same but also in this case the values predicted by the model are shifted forward in time. The MATLAB model shows a different behavior from the experiment around the values ± 0.02 V where the profile tends to slightly flatten this difference is in correspondence of the plateaus of the currents.

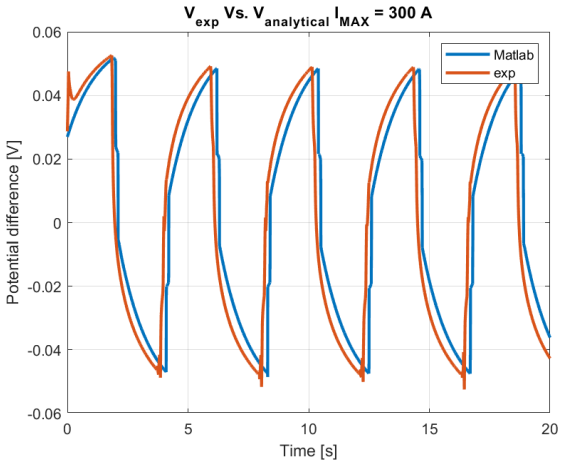


Figure 4.2: Comparison between the experimentally evaluated electric field and the magnetic field predicted by the lumped-parameters method in the case of peak current of 300 A.

Figure 4.3 shows a bar plot where the energy losses per cycle of the actual experiment are compared to the ones predicted by the model. The experimental losses are equal to 5.08 J while the losses in the model are equal to 4.67 J of which 0.35 J derive from the tape while the remaining part is due to dissipation in the copper supports.

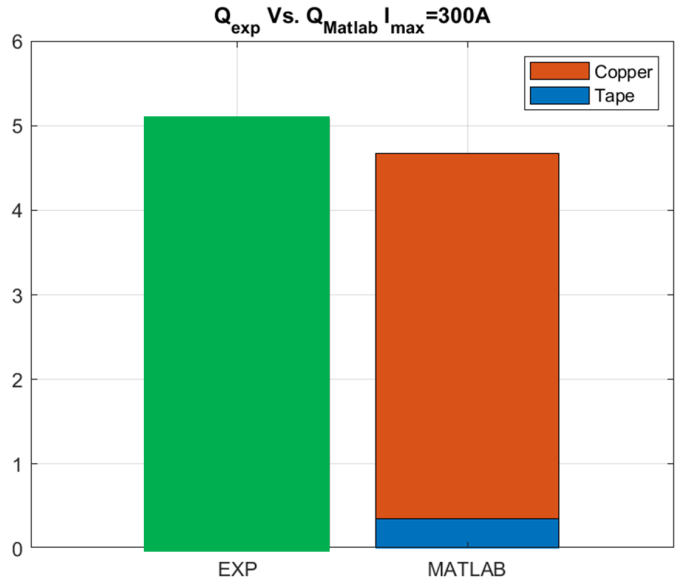


Figure 4.3: Comparison between the experimentally evaluated dissipated energy and the energy dissipation according to the lumper-parameters method in the case with peak current of 300 A.

4.4.2 Maximum current 400 A

Similarly to what was observed in the previous case, the magnetic field of the model is shifted forward in time and in the first instants it has negative values (figure 4.4).

The comparison between the modeled potential difference and the experimentally measured one shows that the two profiles are practically coincident (figure 4.5). This is due to the fact that many parameters of the model were tuned using this experiment as a reference.

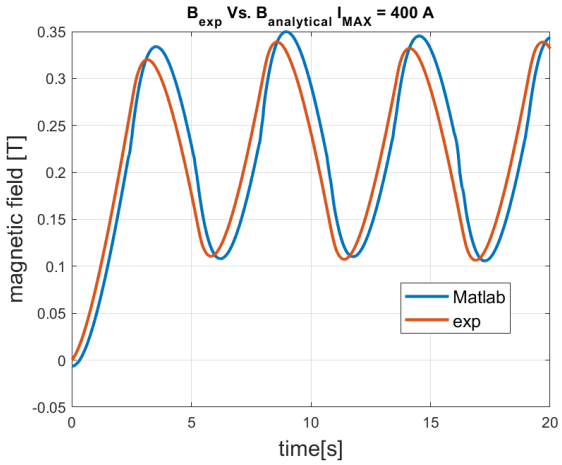


Figure 4.4: Comparison between the experimentally evaluated magnetic field and the magnetic field predicted by the lumped-parameters method in the case with peak current of 400 A.

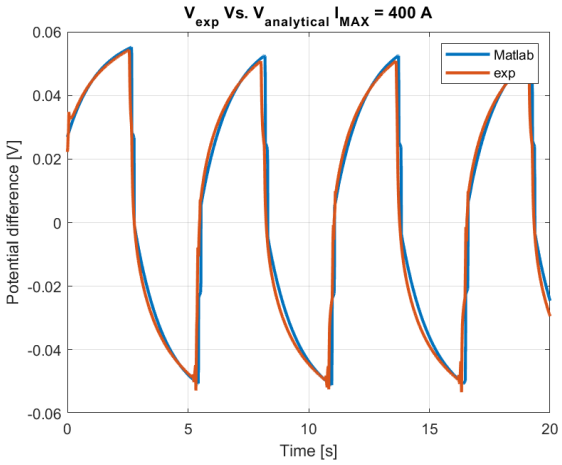


Figure 4.5: Comparison between the experimentally evaluated potential difference and the magnetic field predicted by the lumped-parameters method in the case with peak current of 400 A.

Since the energy lost is the quantity used to tune the unknown parameters the difference between experimental losses and modeled losses is minimal (figure 4.6). The experimental losses are 9.52 J while the modeled losses are 9.84 J of which 1.33 J are dissipated in the tape.

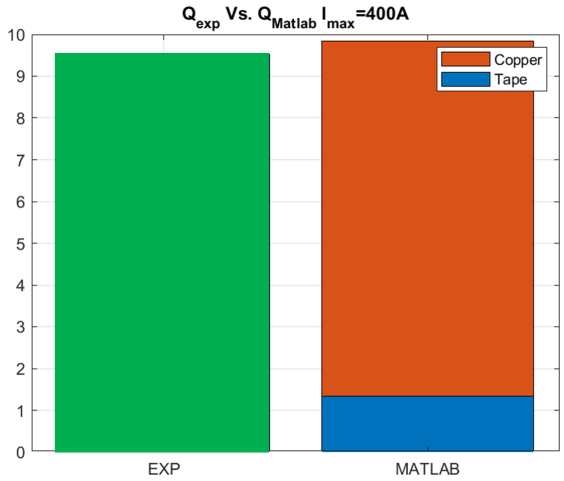


Figure 4.6: Comparison between the experimentally evaluated dissipated energy and the energy dissipated according to the lumped-parameter method in the case of peak current of 400 A.

4.4.3 Maximum current 500 A

In this last experiment the behavior of the magnetic field and of the potential difference (figure 4.7 and figure 4.8) is no significantly different from what was described previously.

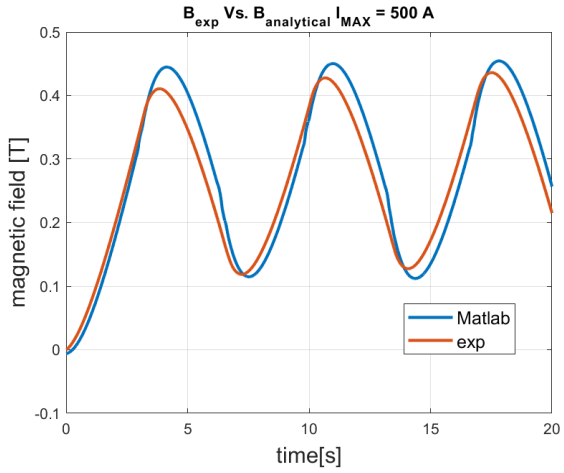


Figure 4.7: Comparison between the experimentally evaluated magnetic field and the magnetic field predicted by the lumped-parameters method in the case with peak current of 500 A.

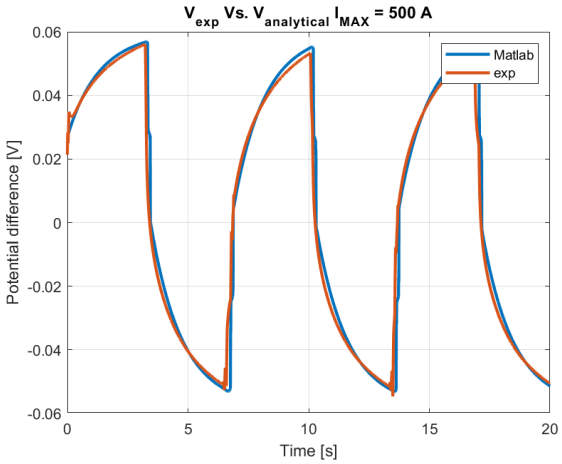


Figure 4.8: Comparison between the experimentally evaluated potential difference and the magnetic field predicted by the lumped-parameters method in the case with peak current of 500 A.

Regarding the energy lost the model is less precise with respect to the other experiments. The losses per cycle in the experiment amounts to 14.55 J while the model predicts a total of energy lost of 16.14 J, giving a difference of more than 10 % between the two quantities.

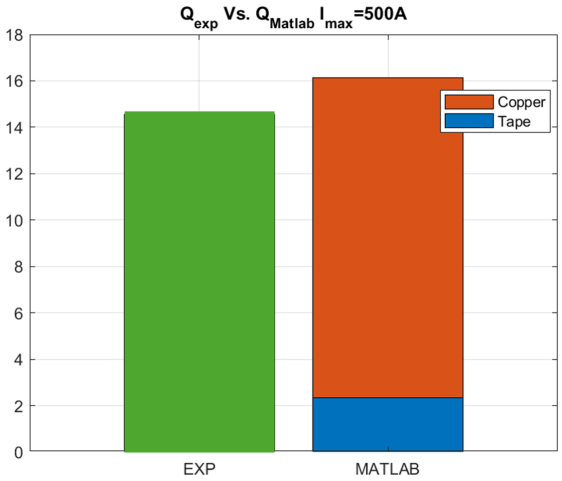


Figure 4.9: Comparison between the experimentally evaluated dissipated energy and the energy dissipated according to the lumped-parameter method in the case of peak current of 500 A.

Finally, for this last experiment, it is shown the contribution to the magnetic field given by each of the three circuits. In figure 4.10 is showed the magnetic field generated from the current flowing in the coil (denoted as B_1), the magnetic field generated by the currents i_2 and i_3 (denoted B_2 and B_3) and the sum of the three contributions that is the magnetic field in the center of the coil according to this model.

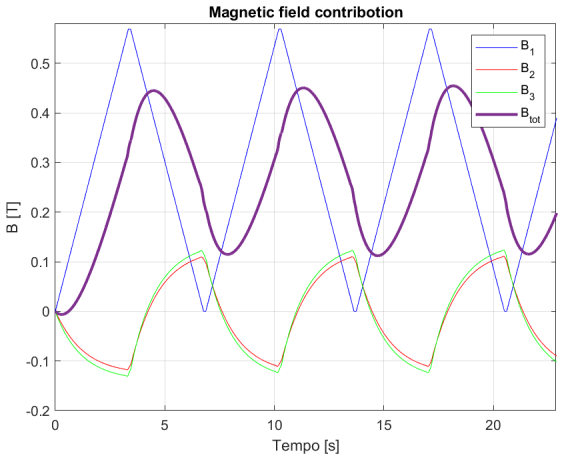


Figure 4.10: Total magnetic field at the center of the system compared with the field generated only by the coil and by the current induced by each of the copper supports.

Chapter 5

Analytical formulations for AC losses

In this chapter, an analytical method for the evaluation of the hysteresis losses in superconductors is compared with the values found numerically in the finite-element simulations. The models analyzed are formulated for simple geometry in simple operating conditions so the comparison with the numerical results cannot be perfect. However, simple analytical formulae like the ones that will be analyzed in this chapter can provide a fast qualitative measure for the hysteresis losses. The main factor that influences the losses is the magnetic field to which the superconductor is subjected. So the first section of this chapter is dedicated to the description of analytical methods to determine its value in the coil cross-section without any numerical tool.

5.1 Analytical method for magnetic field evaluation

To use analytical formulae for the evaluation of the AC losses it is fundamental to know the maximum value of magnetic field to which the coil is subjected. However, the magnetic field to which each turn of the coil is subjected is different from the others. In particular, the innermost turn always sees the highest magnetic field while the outermost turn always experiences a magnetic field in opposite direction with respect of the field in the bore.
According to [18],the variation of the axial magnetic field across the solenoid winding may be approximated with good accuracy by a linear fall-off from $B(r = R_{in})$ at the inner radius to $B(r = R_{out})$ at the outer radius. The values of $B(r = R_{in})$ and $B(r = R_{out})$ are calculated using the equation 4.6; however, that formula diverges

when is exactly at R_{in} or R_{out} so it has to be used at $R_{in} - \epsilon$ and $R_{out} + \epsilon$ using $\epsilon = 10^{-6}\ m$. So the magnetic field in the bore is evaluated using the analytical formula, while the magnetic field in the winding is the linear interpolation of the two values obtained right before the first turn and right after the last one. This method gives a good approximation of the magnetic field but of course it cannot consider the variation of the magnetic field due to the induced currents in the supports, so to take this factor into account the profile of the magnetic field when the maximum current is flowing in the coil is normalized to the maximum of the field experimentally measured in the center of the bore. The results obtained with this method are shown in figure 5.1. It shows the profile of the magnetic field when a current of 500 A flows in the coil, the red line shows the profile obtained with this method normalizing the value in the center to the maximum value measured experimentally ($B = 0.43\ T$) with maximum current 500 and current ramp rate $150/s$. The dashed blue line represents the profile in the same condition evaluated in the COMSOL simulation. The analytical method gives a good approximation of the profile obtained numerically except for the areas close to the extremities of the coil where the formula is less precise. Also in the position $r = 0\ m$ and close to that position the magnetic field of the analytical method is slightly lower than the one of the COMSOL simulation, this happens because the first profile is normalized on experimental value and the numerical simulation overestimates it.

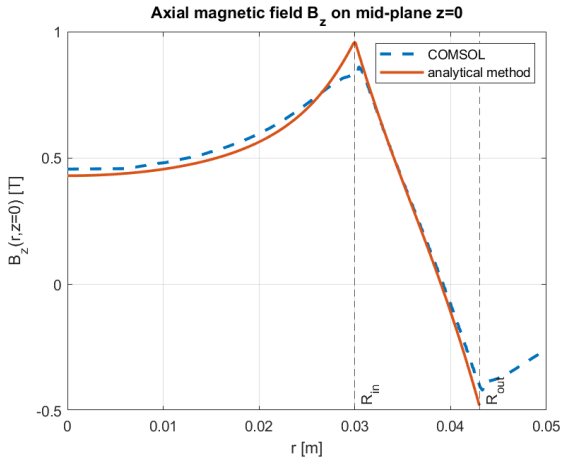


Figure 5.1: Comparison between the magnetic field inside the coil obtained in the COMSOL simulations and the magnetic field evaluated purely analytically.

At this point the maximum value of magnetic field that is reached in a cycle can be estimated. It is obtained by calculating the average across winding of the absolute value of the magnetic field.
The same procedure is done for the other two experiments, the results are shown in table 5.1.

I_{max}	B_{max}
500	0.40 T
400	0.31 T
300	0.23 T

Table 5.1: Average magnetic field in the coil in the three different experiments.

5.2 Hysteresis losses

5.2.1 Kajikawa method

In this section the hysteresis losses produced during the experiments are compared with the formulae presented in [19]. In that paper two formulae are presented to determine the losses of HTS in a varying magnetic field with no transport current. The first method is valid for a superconductor strip while the second is valid for a superconductor slab. The formula for the losses in the strip geometry is the following:

$$W = W_0(2\ln(\cosh h) - h\tanh h) \tag{5.1}$$

The term W_0 is defined as:

$$W_0 = 2\mu_0 J_c a H_c \tag{5.2}$$

In this formula a is the half width of the HTS strip, in this case is 6 mm; J_c is the critical current density in this case it is considered the critical current density of the tape at the maximum field to which the coil was subjected during the 500 A experiment, this value corresponds to a current of 1200 A; H_c is the critical current field, $H_c = J_c d/\pi$ where d is the strip thickness (3.5 μm); finally h is the ratio between the applied field and the critical current field, $h = H_m/H_c$.

The second formula describes the losses of a slab subjected to a varying magnetic field. It is a piecewise function, the definition of the function changes when the applied field overcomes the penetration field H_p, which is defined as $H_p = \lambda J_c a$: a is again the half width of the tape, J_c is evaluated as for the previous case while λ is the ratio between the HTS layer thickness and the spatial interval between two strips, g.

The formula for the evaluation of the AC losses in the slab approximation is equation 5.3. According to the formula the losses are cubic for values of applied field lower than H_p and linear in the case of higher applied field.

$$W = \frac{1}{\lambda} \begin{cases} \frac{2\mu_0}{3} \frac{H_m^3}{H_p} & \text{for } H_m \leq H_p \\ 2\mu_0 H_p H_m \left(1 - \frac{2}{3}\frac{H_p}{H_m}\right) & \text{for } H_m > H_p \end{cases} \tag{5.3}$$

The paper [19] shows that in both cases the AC losses increase with the applied field and that the two models tend to similar results when $H_m/H_c >> 1$. The paper also reports the AC losses evaluated by finite element method of various numbers of HTS strips stacked together at various applied fields. Considering the AC losses of only one HTS strip the paper shows great accordance between the results from the finite element method and the results obtained by the strip approximation. This changes considering more than one HTS strip. Already with a stack of two HTS strips the results from the finite element simulations differ a lot from the results of the formula. As the number of stacked HTS tapes increases, the results via numerical model get closer to the slab approximation.

5.2.2 Comparison with experiments

In this section the formulae previously presented are applied to the experiment analyzed in the previous chapters. The data used in the formulae are reported in table 5.2.

Table 5.2: Parameters used in the experiment.

Parameter	**Value**
Tape width, $2a$	12 mm
Thickness of SC strip, d	3.5 μm
Spatial interval between strips, g	0.20 mm
Critical current density, J_c	2.9×10^{10} A/m^2

The value of g is the spatial interval between two consecutive HTS layers in the pancake so it is the sum of the insulation layer, the copper coating, the Hastelloy and substrate layer, it is evaluated as:

$$g = \frac{(r_{out} - r_{in} - N_{turn}d)}{n_{turn}} \tag{5.4}$$

It had to be evaluated in this way because the thickness of the insulation layer is not constant and cannot be determined directly.

Figure 5.2 shows the result obtained with this approach, in addition to the upper line representing the strip approximation and the lower one that represent the slab

approximation, the blue circles report the hysteresis losses evaluated in the HTS layer by finite elements simulations using COMSOL as described in chapter 3.

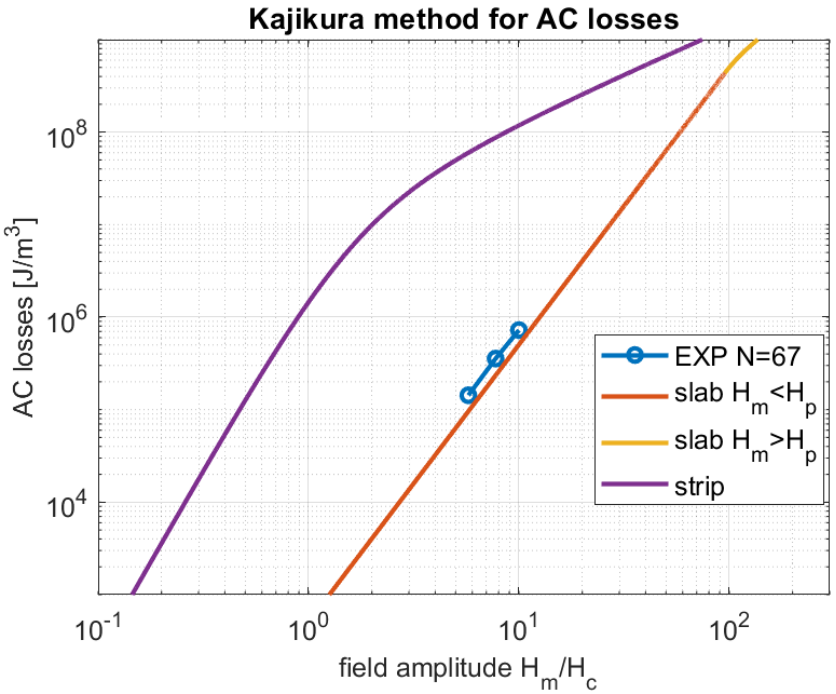


Figure 5.2: Comparison between the analytical formula for the strip and slab geometries and the numerical results from the COMSOL simulation.

Even though the slab approximation seems to closely approximate the results from COMSOL, it has to be considered that the graph has a logarithmic scale that spans many order of magnitude, so actually the difference between the results from the analytical formula and the values obtained with COMSOL cannot be neglected.

Table 5.3: Comparison between simulated data and Kajikara's formula results

Experiment	$I_{max} = 300$ **A**	$I_{max} = 400$ **A**	$I_{max} = 500$ **A**
Hysteresis losses simulated [J/cm^3]	0.143	0.357	0.724
Hysteresis losses from formula [J/cm^3]	0.097	0.240	0.502
Relative error [%]	32%	0.32%	0.31%

The table 5.3 shows the comparison between what was obtained with COMSOL simulation and the results given applying the formula discussed in this section. As it is shown the error between the two cases is around 30% and remains constant among all the cases examined.

Chapter 6

Possible strategy for AC losses mitigation: striated tapes

Rare earth-based coated conductors are at the moment the most promising superconductor technology due to their exceptionally high critical current density and good mechanical strength. In this kind of superconductors the superconductor polycrystalline film is only a couple of μm thick, this means that the tape has an incredibly high aspect ratio (usually around 5000). Large aspect ratio makes the superconductors prone to large AC losses, limiting their use in many practical applications. These limitations include both devices operation in AC mode but also DC magnets which are subjected to varying magnetic field during the ramping of the current. All the theories about the magnetization of superconductors (in particular the ones mentioned in the previous chapter) indicate that the magnetization losses are proportional to the square of the width of the HTS film, therefore a way of reducing the losses is reducing the width of the HTS layer, producing not a continuous HTS film but many filaments. In this way the AC losses could be reduced up to a factor equal to the number of filaments. In this chapter this strategy for the reduction of the losses in superconductors will be analyzed, focusing on how the losses vary when a tape is 'filamentized', when it is an advantage and the methods for the fabrication of this particular tapes. In the following chapter the analysis of the striated tapes will continue presenting some results of some numerical simulations of magnetized tapes.

6.1 AC loss contributions in striated conductors

In order for the striation to be effective in reducing the AC losses it is fundamental that each superconducting striation behaves as a separate object from all the other striations. If the variation of the magnetic field induces currents that couple the different filaments the striation is practically inefficient or can lead to losses even higher than a standard superconductor. To avoid this situation it is important that the space in between the superconducting filament does not contain conductive material that may act as electrical 'bridges'. In the case in which conductive material is present in addition to the hysteresis losses the contribution of the ohmic losses from the current induced in the striation must be added to the global losses.

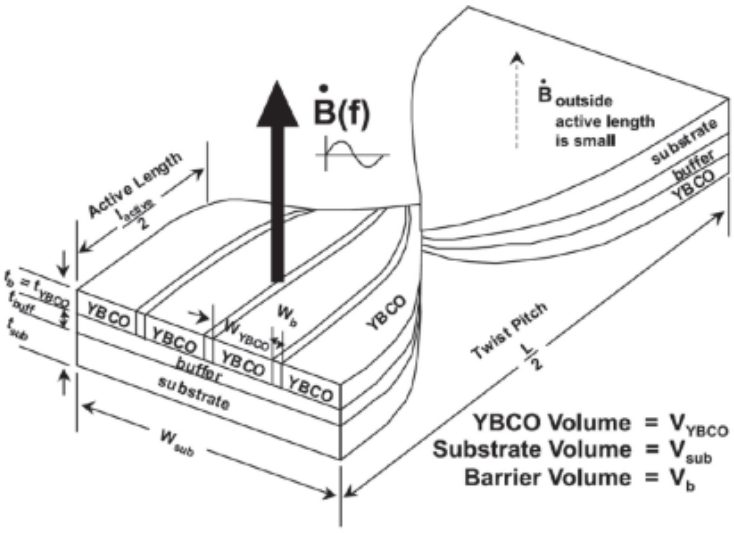


Figure 6.1: Schematic representation of a twisted striated HTS tape under varying magnetic field.

Another possible source of coupling between filaments, even if they are perfectly insulated from each other, is represented by the fact that all the filaments are electrically connected to the current leads that inject the transport current. A possible strategy to uncouple the filaments might be transposing the filaments by twisting them. The same approach is widely used in Low Temperature Superconductors (LTS) but being LTS made in wires the mechanical problems induced by the twisting are much easier to deal with compared to HTS tapes. In this section the different sources of losses and some formulae are reported to easily divide the different contributions.

6.1.1 Hysteresis losses

Hysteresis losses are caused by the penetration and movement of the magnetic flux in the superconductive material. According to [20] the magnetization losses in a thin superconductive strip of width $2a$, thickness $2b$, critical current density per unit of width (sheet critical current density) J_{cs} subjected to a perpendicular field $H_a \sin(\omega t)$ are given by the following formula:

$$Q_{STRIP} = 4\mu_0 a^2 j_{cs} H_a g(H_a/H_c) \quad (6.1)$$

In this formula $g(x)$ is a complex formula that depends on the ratio between the applied magnetic field and the value of critical field H_c defined as $H_c = J_{cs}/\pi$. The formula for the $g(x)$ function is defined as follows: $g(x) = (2/x)\ln(\cosh(x)) - \tanh(x)$.

At large field amplitude $H_a >> H_c$ the expression can be approximated as:

$$Q_{STRIP} = 4\mu_0 a^2 j_{cs}(H_a - 1.386 H_c) \quad (6.2)$$

Both of these formulae give the result in J/m.

another approach proposed in [21] defines the approximated power loss per unit of volume (J/m^3) as:

$$Q_{STRIP} = 2\mu_0 a j_c H_a \quad (6.3)$$

This approximation is valid when the applied field is much larger than the penetration field H_p.

$$H_p = j_c(\frac{2b}{\pi})(\ln\frac{a}{b} + 1) \quad (6.4)$$

Expression 6.1 demonstrates that the hysteresis losses are proportional to the width of the strip squared. So by dividing the $2a$ width into N filaments, each of width $2a/N$ (not considering the narrow space in between the filaments) leads to an AC loss reduction of a factor N. This is actually the case if the field is large enough to fully penetrate the superconductor width, if the field does not fully penetrate the superconductor the advantage of the striation can be lost. The expression to get the hysteresis power losses P_H in W/m it is needed to multiply the last formula reported times the strip cross section ($4ab$) and times the frequency (f) at which the magnetic field varies. Then, by replacing the strip width with the filament width, one obtains the power losses for a striated tape

$$P_H = w I_c B_a f \quad (6.5)$$

In this expression w is the width of the filaments, and I_c is the critical current of the non- striated tape so any degradation of the critical current due to the striation process is neglected.

6.1.2 Eddy-current losses

The variation of the magnetic field does not induce currents only in the superconducting layer but also in the metallic layers, which are electrically conductive. These currents, flowing in an ohmic conductor, generate ohmic losses. The expression for the eddy current power losses per unit volume is[22]:

$$p_e = \frac{\pi^2}{6}\frac{w_s^2}{\rho_s}(B_a f)^2 \tag{6.6}$$

In this expression w_s represents the width of the metallic part and ρ_s its resistivity. Usually this contribution is negligible in the substrate of the tape since the alloys from which it is made have a high resistivity, but it cannot be neglected in the copper stabilizer coating. Interestingly, this term increases when the resistivity of the metallic part decreases, this is due to the fact that with a lower resistivity the induced currents will be much higher. It must be noted that this term, differently from the term related to the hysteresis losses (P_H), depends on the square of the term ($B_a f$).

6.1.3 Coupling losses

The coupling losses are those caused by the currents coupling two or more superconducting filaments via the normal metal regions separating them. With this term we refer to the losses induced by current loops going from a superconductive filaments to another passing through a metallic region. The coupling power loss per unit volume is [23]:

$$p_c = \frac{(fLB_a)^2}{4\rho_\perp} \tag{6.7}$$

In the formula L is the length of the tape and $\rho_\perp$ is the effective transverse resistivity, it depends on the materials that the current crosses in the metallic region between the superconducting ones. As for the eddy-current losses, the coupling losses increase when the effective transverse resistivity decreases, this gives a mathematical explanation to the fact that the striation process gives a proper advantage only if the striations are effectively insulated. Also in this case the losses are proportional to the square of the term ($B_a f$).

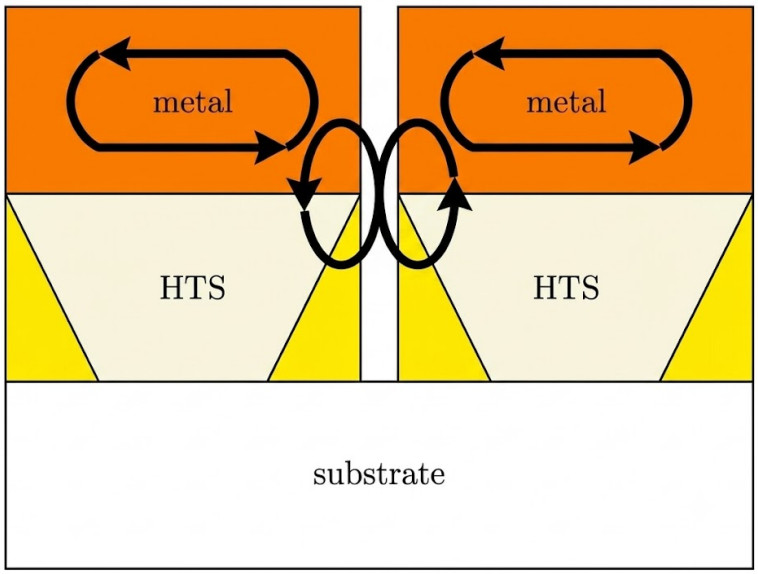


Figure 6.2: Schematic representation of the eddy losses and coupling losses. The first ones are represented by the loops in the metallic region, while the second ones are represented by the loops crossing the superconductor and the metallic stabilizer.

The total losses are given by the sum of the hysteresis, eddy-current and coupling losses, $P_{TOT} = P_H + P_E + P_C$. In this form the total losses can be expressed as power losses per unit of length, per unit of critical current and per unit of sweep rate $B_a f$. To get this expression the formula for P_{TOT} must be divided by the term $I_c f B_a$.

Expressing the losses in this form clearly shows the linear dependence between the total losses and the sweep rate. To simplify the expression the filament width w will be called λ_1 and the term that multiplies $B_a f$ will be called λ_2.

$$\frac{P_{TOT}}{I_c f B_a} = \lambda_1 + \lambda_2 (B_a f) \tag{6.8}$$

By measuring the losses in this form it should appear that the coefficient λ_1 should be equal to the striation width, this is true if the degradation of the critical current due to the striation process is negligible . In addition, the value λ_2 can be used to determine the influence of the eddy-current and coupling loss on the overall power losses. If the striation are actually uncoupled and each filament behaves as a separate object from the others the slope λ_2 will be null and the relation between P_{TOT} and the sweep rate will simply be a horizontal line. On the other hand if the striation are not perfectly insulated the slope λ_2 will be different from zero leading to an increase of the losses when the value $B_a f$ increases [24].

6.1.4 Critical length

As it appears from the formula for the coupling losses they depend on the length of the HTS tape. In particular, in this section a simple formula will be derived for the maximum length for which the coupling losses are negligible. This derivation comes from [18] and it refers to two slab geometry of superconducting material with in between a slab of metal with a varying magnetic field (B_a) perpendicular to the finite side of the slabs. A sketch of the geometry is reported in figure 6.3. The practical case of an HTS tape subjected to a varying magnetic field is very different from the slab approximation: the thickness of the HTS layer is in the order of magnitude of the μm. However, as it will be showed later, some qualitative results can be obtained also with this derivation.

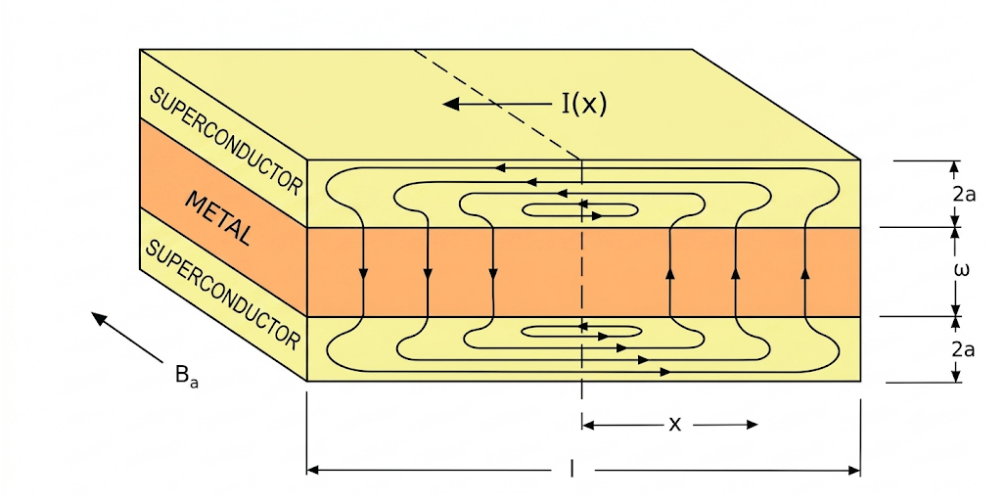


Figure 6.3: Screening currents induced by a varying magnetic field in two slabs of superconductor in contact with a slab of metal.

Let us consider a sandwich of normal conductors in between two slabs of superconductors. When a varying magnetic field is imposed as showed in figure 6.3 currents will be induced in such a way to screen as much of the sandwich as possible from the changing field. It is assumed that the magnetic field has been changing with an amplitude B_a and a frequency f for a long time so that any transient has died and that the field amplitude and frequency are constant everywhere. The current per unit distance at a distance x from the center of the system is called $I(x)$. Across an incremental segment between x and $x + \delta x$, a fraction of this current, δI, crosses the copper matrix to reach the opposite slab. This transverse current flow is driven by the induced voltage $\dot{B}wx$, where w is the thickness of the copper layer. This gives the following result:

$$\delta I(x) = \frac{\dot{B} w x \delta x}{\rho w} \tag{6.9}$$

Solving the differential equation and imposing $I(l/2) = 0$ as boundary condition:

$$I(x) = \frac{\dot{B}(l^2/4 - x^2)}{2\rho} \tag{6.10}$$

So the maximum of the current will be in position $x = 0$. The current per unit of length will fill the whole cross-section at that point when it will be equal to the critical current density (J_c) times the superconducting slab thickness ($2a$). This condition occurs when, given a certain metal resistivity, critical current density and magnetic field variation per unit of time, the length of the tape is equal to the critical length:

$$l_c = 4\sqrt{\frac{a\rho j_c}{\dot{B}}} \tag{6.11}$$

When the length of a tape is longer than L_c it will saturate in the central region and the individual striations will behave more like a single object. To give an approximated value of L_c some characteristic value of each of the involved quantities at 77 K will be considered: the critical current density is set to $J_c = 10^{10}\ A/m^2$, for the copper resistivity $rho(77K) = 2 \times 10^{-9}$
$ohmm$, the rate of change of the magnetic field $\dot{B} = 1\ T/s$ and for the filament half width $a = 0.17\ mm$. This last value is obtained considering a 4 width tape divided into 12 filaments neglecting the loss of superconducting material. Applying the formula with the reported values a critical length of around 23.1 cm is obtained. Of course such a short length is insufficient in any real application, for this reason this length is considered also as the required twist pitch for twisted cables.

6.2 HTS striated tapes fabrication

There are different techniques for dividing Coated Conductors into filaments, most of them can be generally divided into two main groups: striation after or before REBCO synthesis. The first family of methods is more common but has the drawback of losing some superconducting material during the process.

6.2.1 Striation after REBCO

The usual commercial Coated Conductors have the following structure:

- a metallic and flexible substrate, usually made of Hastelloy;

- a thin layer of insulating material, usually MgO. It is needed to guarantee that the crystals of the superconductor are all oriented in the same direction;
- the superconducting layer itself, usually it has a thickness between $1\mu m$ and $3.5\mu m$;
- a thin layer of silver, it is needed to avoid a direct contact between the copper of the coating and the superconductor layer, it is used silver because differently from copper does not chemically react with the superconductor.

This family of techniques consists in removing very thin grooves of silver and superconductor when they were already deposited on the substrate. This process can be done mechanically or by using particular lasers. In the latter case a laser delivers energy to the tape in a short impulse of time. The energy is delivered in such a small interval of time that both the silver and the superconductor are vaporized. The laser passes multiple times on each striation (up to 20 - 40 times) in this way the groove will be more defined but also wider (meaning that more superconducting material is lost). During the process a constant flow of gases is applied, the gas is usually air or Argon (Ar) since it is chemically inert. It is done because the gas flow can remove small particles vaporized by the laser. This technique has many advantages being very precise and easy to scale to an industrial level. However, the intense heat applied by the laser may degrade the side of the superconductor degrading its critical current. another important drawback is that once the substrate or the silver is melted it can be splashed somewhere else in the groove creating an electrical short circuit between filaments that causes high coupling losses, reducing the effectiveness of the striation. To reduce this effect it was proposed to expose these conductors to a oxygen rich atmosphere in order to create oxides on the groove sides that have a high resistance.

another possibility is the mechanical removal of the silver and HTS layer by means of a thin tip that applies a constant load on the tape while it flows under it. This method is quite simple to implement and cheap, also it does not use any heat source so the HTS cannot be degraded. However, the grooves usually are bigger than the ones created with other methods and applying a highly concentrated load on the tape increases the risk of delaminating the tape.

6.2.2 Striation before REBCO

In this family of techniques the striation is done before the deposition of the superconductor so it is usually done on the Hastelloy substrate or on the MgO layer.

One possible strategy is to mechanically remove some material creating the grooves before the deposition of the HTS. In this way when the REBCO is deposited

it will not have the MgO layer in the groove areas and so the REBCO in those areas will be in direct contact with the Hastelloy, the superconductor will grow in a disordered way losing its properties.

6.2.3 Current redistribution in striated tapes

Perfect uncoupling between each filament is desirable to mitigate coupling losses. However, the complete absence of connections between the different filaments might be dangerous for the current-transport capability of the tape. Basically if a single defect appears on only one filament, this filament might be completely unable to transport current if it has no connection with the adjacent filaments. This situation is shown in figure 6.4.

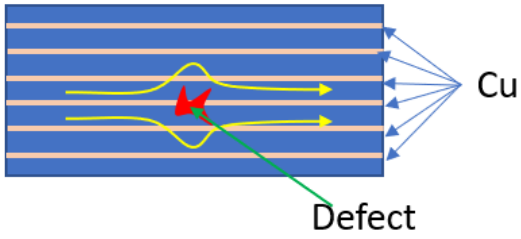


Figure 6.4: Redistribution of the current in a striated HTS tape when it meets a local defect.

To redistribute, the current must cross metallic layer that create ohmic losses that can further damage the tape in that location. To avoid this phenomenon in most HTS striated tapes the filaments are not as long as the overall tape length, but there are some specific location in which the metallic layer in between the filaments stops and the filaments are connected via a small superconducting 'bridge'. In this way if a filament presents a defect the current can bypass the defect crossing one of these bridge and redistributing in the rest of the tape, once overcome the defect can cross another bridge and go back on the original filament. In this only, the degraded part of the filament is a lost. Of course creating connection between the filaments can in principle create coupling between the filaments, so the distance between two consecutive bridges must be long enough not to strongly couple the filaments but at the same time not too long to let the current redistribute properly.

The simplest possible bridge pattern is the so called 'fishnet pattern'. A scheme of this pattern is reported in figure 6.5. A problem of this configuration is that the bridges are all at the same height so the filaments will not couple only with the adjacent one but with all the filaments of the tape.

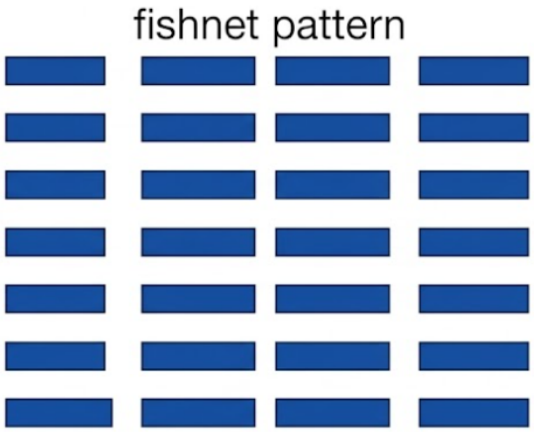


Figure 6.5: Schematic representation of the fishnet pattern used as bridge in striated HTS tapes.

A different configuration that tries to reduce the number of coupled filaments is the 'brick-wall pattern' (figure 6.6). In this pattern the bridges are not all at the same height but staggered. In this way the current crossing the bridge can couple only the filaments close to each other.

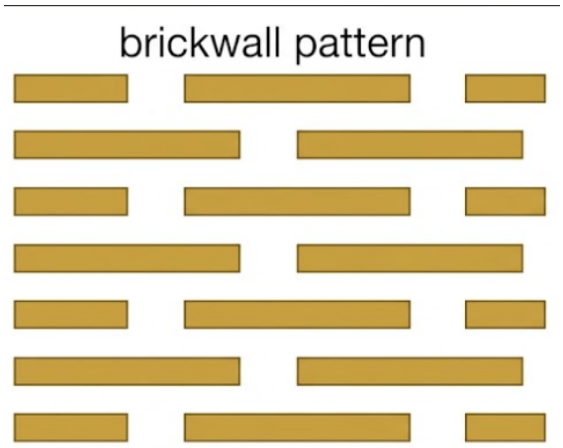


Figure 6.6: Schematic representation of the brickwall pattern used as bridge in striated HTS tapes.

Chapter 7

Case study: Subra HTS striated tape

In this chapter a specific HTS striated tape will be analyzed, the tape is a 4 mm wide tape fabricated by Subra. The striated tape will also be compared with the same without striation. the analysis will focus specifically on the particular fabrication method, the comparison of the critical current between the striated and non-striated conductor, finally the result of some numerical simulations on the losses when both tapes are subjected to a varying magnetic field will be presented.

7.1 Fabrication method: the 2LUPS technique

The tape that will be analyzed was striated using an innovative method different from the ones presented previously. The method is called Two-Level Undercut-Profile Substrate (2LUPS) and can be inserted in the family of striation before REBCO. The main characteristic of this method is that the Hastelloy substrate is structured on two different levels, an upper plateau and a lower one. The tape profile alternates upper and lower plateaus. In particular, the upper plateaus are done in such a way that they slightly stick out with respect to the lower plateaus creating a small shadow area in the region beneath it. A scheme of this structure is reported in the figure below (7.1).

7.1.1 Fabrication steps

The fabrication of the tape consists in several steps [25]:

- The starting point, as for all the striation before REBCO techniques, is a Hastelloy tape. This tape is electrochemically polished using a H_2SO_4 solution

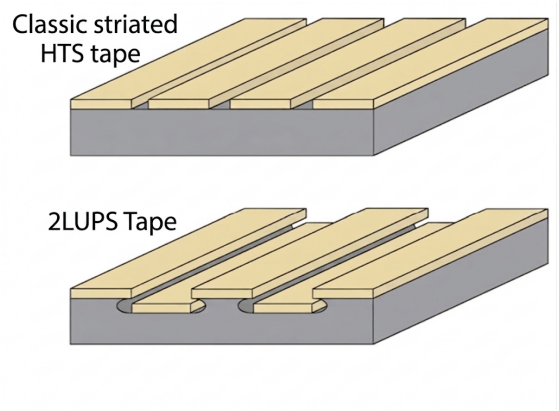


Figure 7.1: Comparison between a standard striated HTS tape a one made with the 2LUPS method. It highlights that the 2LUPS technique better exploits the tape width.

and by applying a low current density across the tape. This process is meant to create a smooth surface.

- At this point an adhesive protective film is placed on the tape.
- The protective film is divided with mechanical cuts in the direction parallel to the rolling direction of the tape. The number of cuts is equal to the number of striations wanted, in this case 12.
- The adhesive film on every second film strip is peeled off and the tape is etched by the same solution used to first polish the Hastelloy. This creates the lower plateaus.
- Now also the remaining protective films are peeled off. At this point the Hastelloy substrate has the desired shape.
- A thin layer of Yttria-stabilized Zirconia (YSZ) is placed on the Hastelloy, followed by a thin layer of CeO_2. These layers take the place of the MgO layer present in most HTS Coated Conductors.
- Only at this point a $1.5\mu m$ layer of YBCO is deposited. It is then covered by a protective silver layer.

7.1.2 2LUPS advantages

The 2LUPS method requires more steps than other processes increasing the complexity and the cost. However, it presents some significant advantages:

- the main advantage is that the area on which the superconductor is deposited remains very close to the area of the tape without striations. This is possible because having two levels on which the YBCO is deposited the filaments are separated by a very small and vertical gap. In this way the reduction of superconducting material is minimal and the critical current of the tape is preserved.

- An other advantage of this method is that it avoids any mechanical or thermal stress on the superconductor.

- This method should also intrinsically guarantee a decoupling between the filaments, this occurs because the substrate on the upper plateau is slightly curved in this way a shadow effect is present that physically separate the filaments on the upper and lower plateaus.

7.2 Critical current comparison

The critical current of both the striated and reference (non-striated) tape is measured to evaluate its reduction due to the striation process. The data obtained with these experiments have been used in the simulations that will be presented in the next sections.

7.2.1 Critical current measurement: experiment

The experiments were performed at the temperature of $77K$ in liquid nitrogen. Figure 7.2 shows the experimental set-up used to perform the experiments. The blocks of copper on the side of the tape are used to inject the current in the sample. It is important that they are large because in this way the current is injected in the sample uniformly, to further increase the uniformity of the current injection some small indium foils were placed between the sample and the copper blocks, being the indium a very ductile material it guarantees a good contact between the sample and the copper. The large copper braids are used to obtain the required current from the power supply.

The experimental setup before being immersed in liquid nitrogen is showed in figure 7.2.

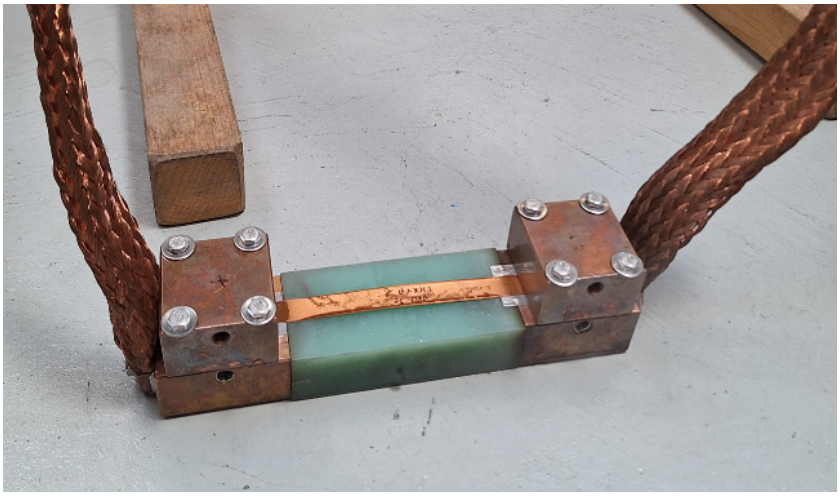


Figure 7.2: Experimental setup for the critical current measurement, on the tape side the copper blocks act as current injection. The set up will be placed in liquid nitrogen to perform the experiment.

The samples of the tape were cut of a length of approximately $20cm$, around $3 - 4$ cm per side were placed under the copper blocks. Two voltage taps were placed at 9.4 cm from each other to collect the potential difference generated across the sample by the current flow. It is important to place the voltage taps quite close to the areas of current injection because they are where the sample most probably will quench. Each critical current measurement is performed twice once with a current ramp rate of 1 A/s and a second time with a current ramp rate of 5 A/s. This double measurement must be done to verify that the result is independent from the current ramp rate.

7.2.2 Critical current measurement: results

To determine the critical current of each sample the potential difference recorded in the experiment is divided by the distance of the voltage tapes. In this way it is obtained the electric field.

After this the obtained data are imported in a Matlab script. The first thing that the script does is filtering the data: removing the data corresponding to currents lower than 10, in that region the oscillation of the electric field are much higher. Now it is defined a personalized function that gives the electric field, with as independent variable the current and with two free parameters to optimize. The function is defined according to the power law as follows:

$$E(I) = E_c(\frac{I}{I_c})^n \tag{7.1}$$

The value of the critical electric field, E_C, for HTS is conventionally set to $100\mu V/m$. At this point, the Matlab function fit finds the combination of free parameters (I_c, n) that minimize the difference between the theoretical curve and the experimental one. The function fit needs the to have an interval for each free parameter in which the function looks for the best-fit value. For the $n - value$ this interval is set between 15 and 40, for the critical current between the 90% and the 60% of the maximum current recorded in the experiment. The critical current of each tape by definition is the current value for which the electric field equals the critical one.

The results of the fitting process for the striated and non-striated tape are reported in the following graphs:

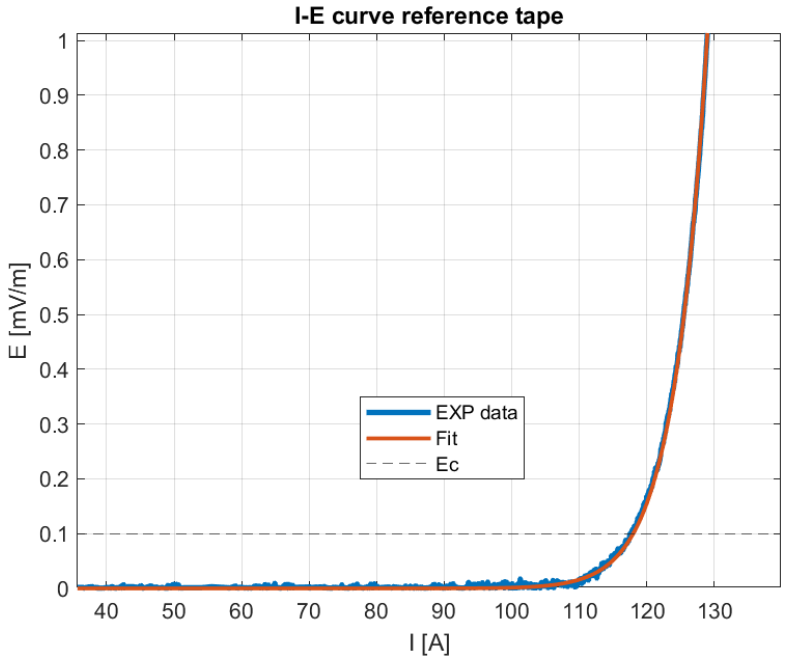


Figure 7.3: Results of the critical current measurement of the standard tape. Comparing the experimental results with the best data fit.

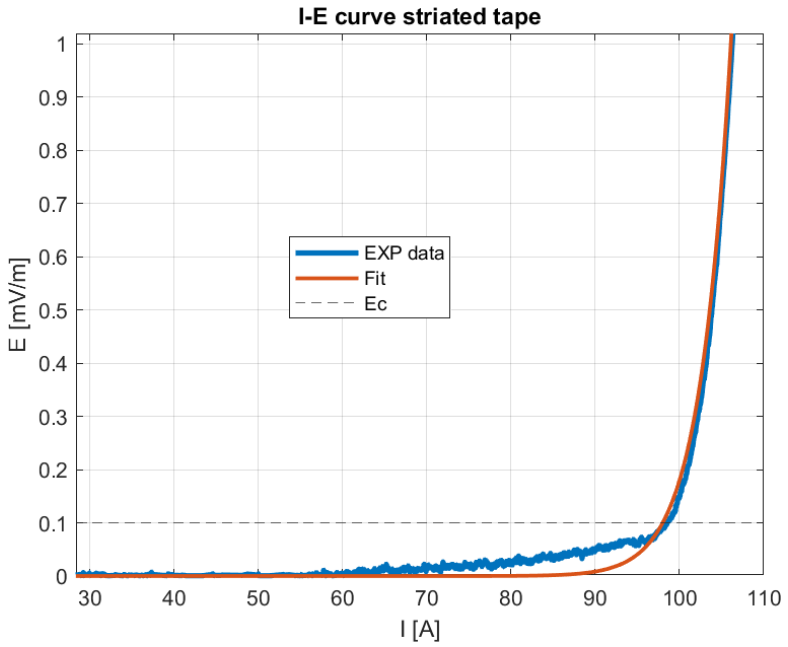


Figure 7.4: Results of the critical current measurement of the striated tape.

The result of the critical current and n-value are reported in the table below:

	Reference tape	Striated tape
Critical current	$118A$	$98A$
n- value	26	29

Table 7.1: Critical current value and n-value for both the reference and striated tape.

The striated tape shows a critical current that is 83% of the reference tape.

Except for the different in critical current the two curves look quite similar, both can be reproduced quite effectively by the power law. However, one significant difference appears for current values immediately lower than the critical one. While in the reference tape the experimental data always follow almost perfectly the fit curve, in the striated tape for the values of current between $60A$ and $90A$ the experimental date diverges from the fitting curve and the electrical field increases linearly. This might be a sign of the current redistributing in different filaments and so crossing some metallic layers. In any case, after the critical current the shape of the experimental data goes back to the expected exponential trend.

7.3 Striated tape: numerical simulations

In this section the results of some numerical simulation made with the software COMSOL will be presented. The simulations will compare the reference and the striated tape when subjected to a varying magnetic field in the direction perpendicular to its width. The striated tape will not be simulated with its complex 3D shape characteristic of the 2LUPS process. Instead, the geometry of the striated tape simulated is simply an alternation of 12 superconducting and 11 metallic filaments. The width of the superconducting and metallic filaments is determined based on the ratio between the critical current of the striated tape and of the reference one. It means that it was assumed that the superconducting material in the striated tape is the 83% of the superconductor in the reference case, this number is exactly the ratio between the two critical currents.

7.3.1 Simulations setup

The simulations were all 3D and reproduced only the superconducting layers and the striations. It means that all the other layers composing a coating conductor were neglected. In the reference case only a $2\mu m$ thick layer of YBCO was modeled, while in the striated case it was modeled the superconducting filaments alternated with metallic filaments both with the same thickness of $2\mu m$. Obviously, simulating only part of the tape it is only possible to reproduce the hysteresis losses and the coupling one; the eddy-current losses will be neglected.

In the reference case the geometry simulated is a parallelepiped $2mm$ long, 2 mm width and 2 μm thick, around it there is a quarter sphere of radius 5 cm. The geometry of the striated tape consisted in 12 superconducting filaments divided by 11 copper striations; the superconducting filaments are $2mm$ long 2 μm thick and have a width of 0.28 mm. The copper striations have the same length and thickness but a width of 0.06 mm. These dimensions were chosen to obtain a ratio between the superconducting width and the total one equal to the ratio between the critical current of the striated tape and the reference one. The simulation uses the $H - \phi$ method and is based on the work present in [26]. The H formulation is used to model the extremely non-linear superconductive domain and the ϕ for the air volume around the tape. The H formulation is also being used for the copper striation in the striated tape. To reduce the computational domain the symmetry of the problem was exploited, imposing the zero flux constraint on the inner sides of the quarter of the sphere and the inner sides of the parallelepiped. In this way, what was actually simulated was a 4×4 mm parallelepiped. On the other surfaces the boundary conditions imposed were used to impose the continuity of the magnetic flux between the two formulations on the surfaces on the boundary between the two domains; and on the curve part of the quarter of sphere it was

imposed a Dirichlet boundary condition to impose the exciting filed perpendicularly to the wider face of the HTS sample.

The exciting field follows a triangle wave that varies between $0.05T$ and $-0.05T$ and it completes a cycle in $0.667ms$.

To properly mesh the computational domain it was used a tetragonal mesh for the air domain and a mapped mesh for the HTS sample. In the reference simulation the superconductor presented one element over the tape thickness and 100 elements in the other two dimensions. The striated tape was meshed with one element for the tape thickness and 100 elements for the tape length while each superconductor filaments is meshed with 10 elements on its width, each copper striation width was mesh with 2 elements.

7.3.2 Results

The simulations done analyzed three different cases: a $4X4$ mm of striated tape with highly insulated striations, a $4X4$ mm of striated tape with striation made only of copper and a sample of tape made with the same width but with length equal to the critical one. Each simulation is compared with the non striated tape, for each simulation it will be reported the ratio between the energy dissipated in the reference case and in with the striated tape and the plot of the current density in the sample. Firstly, it is presented the current density distribution in the case of a non-striated tape:

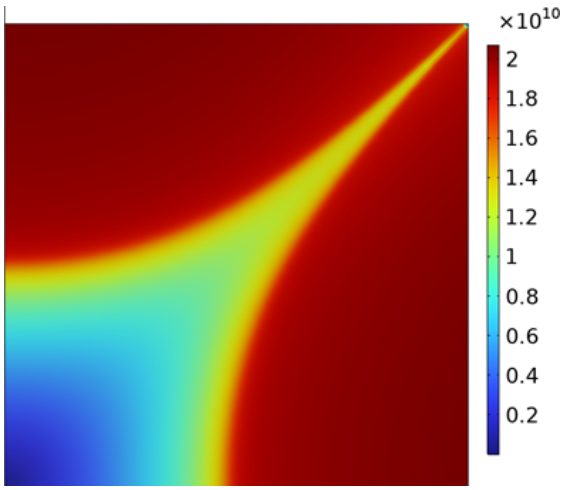


Figure 7.5: Current density distribution in one quarter of the non-striated $2X2mm$ sample when the peak field is applied.

In the case of highly insulated striation it was used a resistivity 25 times higher the one of copper at $77K$ ($\rho_{str} = 25X2 \times 10^{-9}$ Ωm). The ratio between the energy

dissipated in the reference casa and in this case is:

$$\frac{Q_{ref}}{Q_{str-ins}} = 12.2 \tag{7.2}$$

This value is in good agreement with the expectation. The fact that the ratio is even higher than the number of turns is due to the finite length of the sample. In fact, the assumption that the ratio of the dissipated energies is equal to the number of striation is valid only considering an infinite length.

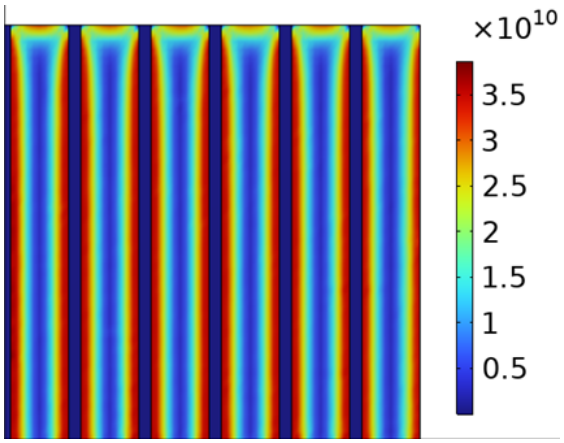


Figure 7.6: Current density distribution at peak field, in this case the striation have a resistivity $\rho = 25\rho_{Cu}$.

It can be seen that each superconductive filament acts as a completely independent object with respect to the other filaments.

In the case of the 'standard' striated tape, with a resistivity in the striation of $\rho_{Cu} = 2e - 9\Omega * m$ the ratio between reference and striated tape becomes:

$$\frac{Q_{ref}}{Q_{str}} = 4.27 \tag{7.3}$$

This value is far from the previous one because with a lower value of resistivity in the striations current can cross them and it generates ohmic losses. The total amount of coupling losses in this case is the 70% of the total.

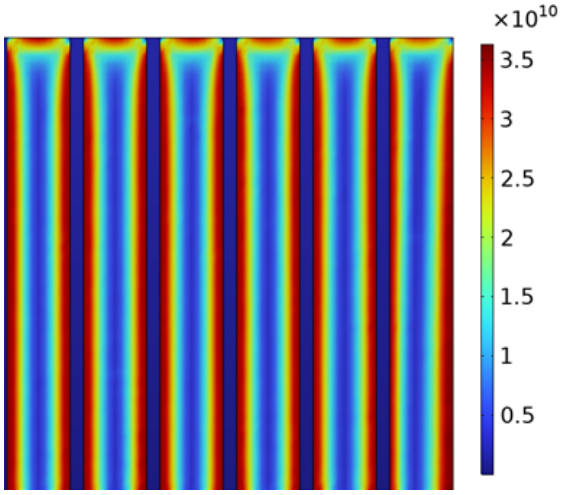


Figure 7.7: Current density distribution in the case of striated tape with resistivity in the striation equal to the one of copper.

The current density distribution seems equal to the one obtained in the previous case, but in this case looking at the most external filament it is possible to see some differences with respect to the other. In that filament the current on the left side and on the right one are not equal, the imbalance between the current on the two sides means that the current loops are not closing inside that striation but they cross the copper striation to close.

In the final case a tape 16 mm long was analyzed. This value is the one obtained as critical length according to the formula presented in the previous chapter. In this case obviously the dissipated energy is compared with a non striated tape of the same length. The ratio of dissipated energy between this two cases is:

$$\frac{Q_{refL_C}}{Q_{strL_C}} = 1.05 \tag{7.4}$$

As expected this ratio is very close to one, meaning the advantage of the striations is completely lost when the tape length is L_C.

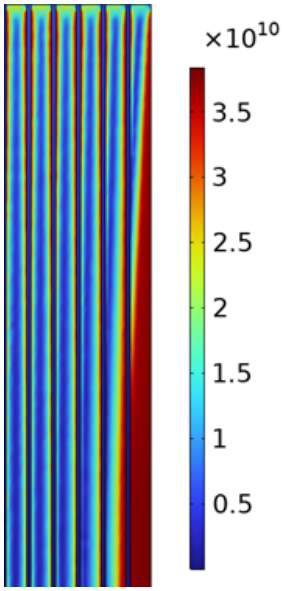


Figure 7.8: Current density distribution in a striated tape of length equal to the critical one.

In this case the current distribution is completely different from the other ones, it can be clearly seen that the striations have an influence on each other and that the current loops do not close inside a single filament.

Chapter 8

Conclusion and Outlook

This thesis presented an investigation into the transient electromagnetic behavior and AC loss mechanisms in High-Temperature Superconducting (HTS) coils, combining experimental results, finite element modeling, lumped-parameter circuit simulations, and advanced conductor mitigation techniques.

8.1 Summary of Main Results

The core outcomes of this research can be divided into two main areas: the analysis of the conduction-cooled pancake coil and the evaluation of striated coated conductors for AC loss reduction.

Electromagnetic Dynamics and AC Losses in the Pancake Coil

- **Dominance of Support Induced Currents:** The experimental campaign on the 67-turn pancake coil carried out at the Paul Scherrer Institute (PSI) revealed significant deviations from the expected magnet behavior, a phase lag and amplitude attenuation in the bore magnetic field relative to Biot-Savart calculations, also the potential difference at the coil terminals and the dissipated power were did not respected the expectations. Numerical modeling in COMSOL Multiphysics (coupling the H-formulation in the superconductor and the A-formulation in surrounding conductive domains) conclusively demonstrated that these phenomena are governed by large induced currents within the copper structural and cooling supports ($RRR = 78.9 \pm 0.3$, characterized experimentally). These currents reach peak magnitudes on the order of 10^4 A, actively screening the magnetic flux variation and generating over 80% of the total cycle dissipation across all tested ramp conditions (300 A, 400 A, and 500 A at 150 A/s).

- **Validation of Numerical and Lumped Models:** The 2D axisymmetric FEM model exhibited quantitative agreement with experimental measurements, accurately reproducing the transient waveforms of both the magnetic field and coil potential difference, with cycle loss predictions closely matching measured values (e.g., 5.13 J simulated vs. 5.09 J measured at 300 A). Furthermore, the 3-circuit lumped-parameter model implemented in MATLAB confirmed that representing the coil and copper supports as mutually coupled inductive-resistive circuits provides a computationally efficient tool capable of predicting the global electrical response of the system.

- **Benchmark with Analytical Hysteresis Formulations:** Comparison between FEM-computed HTS hysteresis losses and the classical Kajikawa analytical formulations indicated that the closely wound pancake geometry approaches the multi-tape slab regime rather than an isolated strip. While the slab model captures the qualitative trend, it systematically underestimates hysteresis losses by approximately 30%, primarily due to the differences in the geometry, the non-uniform field exposure, and the complex trend of the THEVA tape critical current.

AC Loss Mitigation via Striated REBCO Tapes

- **Critical Current Retention in 2LUPS Tapes:** Experimental transport measurements at 77 K on Subra 12-filament striated tapes demonstrated a critical current retention of 83% (98 A vs. 118 A for the non-striated reference tape). This confirms that structuring the Hastelloy substrate prior to REBCO growth via the Two-Level Undercut-Profile Substrate (2LUPS) technique successfully prevents the substantial loss of superconducting cross-section and edge degradation typical of post-deposition laser ablation.

- **Filament Decoupling and Coupling Loss Thresholds:** Three-dimensional numerical simulations using the H-ϕ formulation verified that under adequate inter-filament transverse insulation ($\rho_{\mathrm{str}} = 25\rho_{\mathrm{Cu}}$), the 12-filament tape reduces magnetization losses by a factor of 12.2, in agreement with the theoretical factor N for short samples. However, when standard copper striations are present, inter-filament coupling currents account for approximately 70% of the total dissipation, reducing the loss ratio to 4.27. Moreover, when the conductor length equals or exceeds the critical coupling length ($L_c \approx 16\,\mathrm{mm}$ under the simulated sweep conditions), the loss-reduction benefit is completely lost ($Q_{\mathrm{ref}}/Q_{\mathrm{str}} \approx 1.05$), loosing the advantage of striations.

8.2 Future steps

The findings of this work highlight key guidelines and open challenges for the design of dynamic HTS magnets and low-loss coated conductors:

- **Mitigation of Eddy Currents** To prevent prohibitive cryogenic heat loads in conduction-cooled AC magnets, future structural and thermal support designs must incorporate an appropriate geometry presenting azimuthal cuts, radial slits, or electrically insulating thermal breaks. Such modifications disrupt large induced current loops while preserving the necessary thermal contact surface with cryocoolers or heat pipes.
- **Transposition and Current Sharing in Striated Tapes:** For the practical adoption of multi-filamentary REBCO conductors in long-length windings, filament transposition must be explored. For this reason the study of possible geometry to create a proper HTS twisted cable is needed.

Bibliography

[1] URL: https://www.theva.de/wp-content/uploads/2018/05/171218_THEVA_Broschuere_Pro-Line_generalproperties.pdf (cit. on p. 8).

[2] URL: Hastelloy%20C-276%20(Composition,%20Properties,%20and%20Applications)%20%E2%80%93%20Materials%20Science%20and%20Engineeringf (cit. on p. 8).

[3] E.F. Talantsev et al. «Critical current anisotropy for second generation HTS wires». In: *??* (??) (cit. on p. 9).

[4] W. Prusseit et al. «Working around HTS Thickness Limitations – towards 1000+ A/cm – Class Coated Conductors». In: *??* (??) (cit. on p. 10).

[5] B J H de Bruyn et al. «AC losses in HTS coils for high-frequency and non-sinusoidal currents». In: *??* (??) (cit. on p. 20).

[6] URL: https://doc.comsol.com/6.4/doc/com.comsol.help.acdc/acdc_ug_magnetic_fields.08.110.html#1071877 (cit. on pp. 24, 25).

[7] URL: https://doc.comsol.com/6.4/doc/com.comsol.help.acdc/acdc_ug_theory.05.70.html#741640 (cit. on p. 24).

[8] URL: https://doc.comsol.com/6.4/doc/com.comsol.help.acdc/acdc_ug_theory.05.21.html#746755 (cit. on p. 25).

[9] URL: https://htsdb.wimbush.eu/ (cit. on p. 27).

[10] F. Grilli B. Shen. «Overview of H-Formulation: A Versatile Tool for Modeling Electromagnetics in High-Temperature Superconductor Applications». In: *IEEE Transactions on Applied Superconductivity* (2020) (cit. on p. 28).

[11] J. Lu. «Physical properties of Hastelloy® C-276™ at cryogenic temperatures». In: *??* (??) (cit. on p. 29).

[12] URL: https://webbook.nist.gov/cgi/inchi/InChI%3D1S/Ag (cit. on p. 29).

[13] £. S. Drexler N. J. Simon and R. P. Reed. «Properties of Copper and Copper Alloys at Cryogenic Temperatures». In: *??* (??) (cit. on p. 31).

[14] Hugh W. Coleman et al. «ASME VV 20-2009 Standard for Verification and Validation in Computational Fluid Dynamics and Heat Transfer». In: *ASME* (2009) (cit. on p. 32).

[15] K. Ji et al. «Analysis of Eddy-Current Loss and its Reduction in a Conduction-Cooled HTS Magnet». In: *??* (??) (cit. on p. 43).

[16] Eldward B. Rosa and Frederick W. Grover. «FORMULAS AND TABLES FOR THE CALCULATION OFMUTUAL AND SELF-INDUCTANCE». In: *Bureau of standards* (1916) (cit. on p. 46).

[17] James C. Simpson. «Simple Analytic Expressions for the Magnetic Field of a Circular Current Loop». In: *NASA / TM 2013 -217919* (2001) (cit. on p. 49).

[18] Martin N. Wilson. *Superconducting magnets*. Clarendon press Oxford, 1983 (cit. on pp. 56, 66).

[19] S Awaji K Kajikawa and K Watanabe. «Numerical evaluation of AC losses in an HTS insert coil for high field magnet during its energization». In: *IEEE Transactions on Applied Superconductivity* (2014) (cit. on pp. 58, 59).

[20] Brandt E H and Indenbom M. «Type-II-superconductor strip with current in a perpendicular magnetic field». In: *??* (1993) (cit. on p. 63).

[21] E W Collings M D Sumption and P N Barnes. «AC loss in striped (filamentary) YBCO coated conductors leading to designs for high frequencies and field-sweep amplitudes». In: *??* (2004) (cit. on p. 63).

[22] K.V. Namjosh. «Low-frequency eddy-current loss estimation in long conductors by using the moment of inertia of cross sections». In: *??* (2004) (cit. on p. 64).

[23] Charles E. Oberly. «How filaments can reduce AC losses in HTS coated conductors: a review». In: *??* (2001) (cit. on p. 64).

[24] F. Grilli. «ac Loss analysis for superconducting generator armatures wound with subdivided Y–Ba–Cu–O coated tape». In: *??* (2016) (cit. on p. 65).

[25] A C Wulff. «Two level undercut-profile substrate for filamentary YBa2Cu3O7 coated conductors». In: *??* (2015) (cit. on p. 71).

[26] Alexandre Arsenault, Frédéric Sirois, and Francesco Grilli. «Implementation of the H-ϕ Formulation in COMSOL Multiphysics for Simulating the Magnetization of Bulk Superconductors and Comparison With the H-Formulation». In: *IEEE Transactions on Applied Superconductivity* 31.2 (2021), pp. 1–11. DOI: 10.1109/TASC.2020.3033998 (cit. on p. 77).